arXiv:2510.18663v1 [gr-qc] 21 Oct 2025

Comprehensive analysis of dissipative effects in the induced gravitational waves

Yan-Heng Yu [a,b] **, Zhe Chang** [a,b] **, Sai Wang** [c,*]

[a]Theoretical Physics Division, Institute of High Energy Physics, Chinese Academy of Sciences, 19B Yuquan Road, Shijingshan District, Beijing 100049, China

[b]School of Physical Sciences, University of Chinese Academy of Sciences, 19A Yuquan Road, Shijingshan District, Beijing 100049, China

[c]School of Physics, Hangzhou Normal University, No.2318 Yuhangtang Road, Yuhang District, Hangzhou 311121, China

E-mail: yhyu@ihep.ac.cn, changz@ihep.ac.cn, wangsai@hznu.edu.cn

Abstract. Dissipation is an intrinsic property of the cosmic fluid, leading to the damping of curvature perturbations at small scales. In this paper, we comprehensively study dissipative effects in gravitational waves induced by curvature perturbations, known as induced gravitational waves (IGWs). We find dissipative effects become especially significant at wavenumber $k \sim k_{\mathcal{H},\mathrm{dec}}$, where $k_{\mathcal{H},\mathrm{dec}}$ corresponds to the horizon scale at the decoupling of weakly-interacting particles. They can leave characteristic features on the IGW spectrum, including a notable suppression with a "double-valley" structure at $k \sim k_{\mathcal{H},\mathrm{dec}}$ and a modified infrared behavior without logarithmic running at $k \lesssim k_{\mathcal{H},\mathrm{dec}}$. Within the Standard Model of particle physics, dissipative effects caused by neutrinos at the nanohertz frequencies can be important in the analysis of pulsar timing array data. Furthermore, dissipation-induced features associated with possible new weakly-interacting particles can be detectable by a wide range of gravitational-wave experiments, serving as a promising probe of new physics at extremely high energy scales. As an extension, we also discuss dissipative effects in the presence of primordial non-Gaussianity and their impacts on the anisotropies of IGWs and the poltergeist mechanism. These dissipative effects not only provide a more realistic description of IGWs but also exhibit rich phenomenology and profound physical implications, opening a new window into understanding the early Universe and fundamental physics.

---

*Corresponding author.

Contents

1 Introduction

Understanding the early Universe is one of the central objectives for cosmology and fundamental physics. Gravitational waves (GWs), due to their nature of hardly interacting with other matters, provide a unique window to detect the Universe's earliest epochs, which are otherwise inaccessible to electromagnetic probes. Cosmological stochastic gravitational-wave backgrounds (SGWBs), including those form inflationary quantum fluctuations, preheating, phase transitions, topological defects, and cosmological scalar perturbations, are searched across a wide range of frequency bands. To be specific, ground-based GW interferometers like LIGO, Virgo, and KAGRA (LVK) [1–3] have hunted for the hundred-hertz SGWB and established upper limits [4], space-based GW interferometers like the upcoming Laser Interferometer Space Antenna (LISA) [5] are anticipated to seek the milli-hertz SGWB in the next decade, and, most excitingly, pulsar timing array (PTA) experiments (i.e., North American Nanohertz Observatory for Gravitational Waves (NANOGrav) [6], European Pulsar Timing

Array (EPTA) [7], Parkes Pulsar Timing Array (PPTA) [8], and Chinese Pulsar Timing Array (CPTA) [9]) have already found strong evidences of the nano-hertz SGWB [10–13]. These cosmological SGWBs, once detected, will bring us a wealth of physical information about the early Universe, marking a milestone to explore cosmology and fundamental physics.

Induced gravitational waves (IGWs) [14–20], as an important constituent of the cosmological SGWBs, have garnered substantial attention recently. They exhibit close connections to many crucial problems in the early Universe, e.g., inflation, cosmic evolution, primordial black holes (PBHs), etc., and can also well explain the SGWB reported by PTAs [21]. These IGWs are naturally predicted by the cosmological perturbation theory, referring to the secondary GWs induced by the nonlinear couplings of linear cosmological scalar perturbations ϕ. The production of IGWs is determined by both the primordial curvature power spectrum $\mathcal{P}_\zeta$ and the evolution of ϕ after inflation. While cosmic microwave background (CMB) observations set $\mathcal{P}_\zeta \sim 10^{-9}$ on large scales [22], $\mathcal{P}_\zeta$ is allowed to be large enough to produce observable IGWs on small scales. Particularly, an enhanced small-scale $\mathcal{P}_\zeta$ is also well-motivated by the formation of PBHs, which are one of the leading dark matter candidates. For a given $\mathcal{P}_\zeta$, the IGWs are then determined by the classical evolution of ζ after horizon reentry, which highly depends on the properties of cosmic fluid. Therefore, the IGWs also serve as a sensitive tracer of these properties of cosmic fluid in the early Universe.

The focus of this paper is to discuss the relationship between the IGWs and an inherent nature of cosmic fluid, namely, the dissipation in it. In most existing studies, the cosmic fluid is simply assumed as a perfect fluid without dissipation. This can be a good approximation if the mean free path of particles in cosmic fluid is negligible, leading to a simplified analysis of the evolution of ζ. Based on this assumption, we can establish direct links between the IGWs and the early Universe. The energy-density spectrum of IGWs, $\Omega_{\rm gw}$, in the standard radiation-dominated (RD) Universe can be calculated through a semi-analytical method [18, 19]. Besides, other crucial issues, such as non-standard cosmic expansion history, primordial non-Gaussianity, and GW anisotropies, have also been widely investigated in the study of IGWs, providing deeper insights into the early Universe. So far so good.

However, since the mean free path of particles is non-vanishing in reality, the cosmic fluid essentially has viscosity and thermal conduction, with inevitable dissipative effects in it. In fact, the diffusion of particles from high-density to low-density regions can erase the sound waves in cosmic fluid on scales smaller than a typical diffusion scale k_D^{-1}. As a result, these sound waves for the modes $k \gg k_D$ dissipate their energy with an exponential damping [23]. These dissipative effects, as a universal property of fluid, have important applications in cosmology. The damping in the photon-baryon plasma caused by the photon diffusion is well-known as "Silk damping" [24], which results in the suppression of the CMB angular power spectrum at the multipoles $\ell > 10^3$. Similar dissipative effects due to the particle diffusion generally exist in the earlier Universe, offering valuable insights into small-scale ζ [25]. As for IGWs, since dissipative effects can significantly affect the evolution of ζ, they

should be a basic factor to consider in the study of IGWs.

Though of great importance, dissipative effects in IGWs have long been ignored until recent works. Ref. [26] firstly investigated dissipative effects in IGWs and also named them as "Silk damping". The main effect of dissipation (for a broad $\mathcal{P}_\zeta$) is suppressing Ω_{gw} at the frequencies related to the decoupling of weakly-interacting particles. By revealing the relation between these frequencies and particle interactions, Ref. [26] proposed that dissipative effects in IGWs can be a novel probe to new physics, as an essential complement to particle physics methods. In Ref. [27], the authors concentrated more on the case of a sharply-peaked $\mathcal{P}_\zeta$. In this case, the dissipation modifies Ω_{gw} by regularizing the divergent peak at the resonant frequency and removing the typical logarithmic running in the infrared region. Additionally, semi-analytical methods for some special conditions are developed to calculate Ω_{gw}.

In this paper, we will present a comprehensive and in-depth study of dissipative effects in IGWs. We will start from the particle interactions in the early universe and establish their general relationship with the dissipative effects. In more general cases (different types of $\mathcal{P}_\zeta$ and various dissipation parameters), we will conduct a detailed study on how dissipation influences the IGW spectrum. Our results uncover a rich phenomenology of dissipative effects. Notably, we newly find that dissipation can produce a characteristic multi-valley structure and induce complex modifications to the infrared behavior. Furthermore, we will provide an analysis of the physical origins behind these phenomena. As an extension, we will also explore the interplay between dissipative effects and primordial non-Gaussianity, GW anisotropies, and the poltergeist mechanism. The implications of our work include: (i) Since Ω_{gw} is the most basic observable for IGWs, its precise calculation is essential for GW data analysis. Accounting for the universal and significant role of dissipation, our study offers a more realistic description of IGWs, making it highly important for upcoming GWs experiments. (ii) Identifying the sources of SGWB is crucial but challenging. The dissipation-induced feature on Ω_{gw} offer a powerful way to differentiate IGWs from other GW origins. Especially, dissipative effects from neutrinos are expected to provide insightful insights into whether IGWs can account for the nano-hertz SGWB reported by PTAs. (iii) Dissipative effects in IGWs, especially the newly discovered multi-valley feature, could act as unique signatures of particle decoupling in the early Universe. This can opens the door to extracting valuable insights into fundamental physics at extremely high energy scales.

This paper is organized as follows. In Sec. 2, we establish the theoretical foundation of this work by deriving Ω_{gw} in the presence of dissipation. In Sec. 3, we demonstrate the numerical results of Ω_{gw} for different types of $\mathcal{P}_\zeta$. We also summarize the properties of dissipatives effects and analyze their physical origins. In Sec. 4, we emphasize physical implications of these dissipative effects in IGWs for GW observations and for new physics searches. In Sec. 5, we discuss the dissipative effects in the presence of primordial non-Gaussianity, and how dissiaption affects anisotropies of IGWs and the poltergeist mechanism. Sec. 6 makes a conclusion of our work.

2 Theoretical foundations

2.1 Dissipation in cosmic fluid

We start from considering the hydrodynamic properties of cosmic fluid in the RD Universe. Due to the non-vanishing mean free path of particles, the cosmic plasma should be described as an imperfect relativistic fluid with dissipation, with its energy-momentum tensor being

$$\mathcal{T}_{\mu\nu} = pg_{\mu\nu} + (\rho + p)u_\mu u_\nu + \Delta\mathcal{T}_{\mu\nu}(\eta, \xi, \chi) , \tag{2.1}$$

where $g_{\mu\nu}$ is the spacetime metric, ρ, p, and u_μ denote the energy density, pressure, and velocity four-vector of the cosmic fluid, respectively. The additional small term $\Delta\mathcal{T}_{\mu\nu}$ stands for the deviation from perfect fluid caused by the dissipation, and can be generally characterized by three parameters, namely, the shear viscosity η, bulk viscosity ξ, and heat conduction χ [23, 28]. The presence of $\Delta\mathcal{T}_{\mu\nu}$ modifies the equations of motion of the perturbations $\delta\rho$, δp, and δu_μ, effectively introducing an additional decay rate proportional to k^2, which implies significant damping of small-scale perturbations [23].

From microscopic perspectives, this dissipation originates from the diffusion and thermalization of particles in cosmic fluid . During the RD era, the dominant source of dissipation is the shear viscosity, which is given by the specific particle interactions, i.e., [25, 26]

$$\eta(\tau) \simeq \frac{16}{45}\rho_\gamma t_\gamma + \sum_{j=\nu,X,\,...} \frac{4}{15}\rho_j t_j\, \Theta(\tau_{j,\mathrm{dec}} - \tau) + ... \ . \tag{2.2}$$

Here, for each particle species i, ρ_i is its energy density, t_i is its mean free time, τ is the conformal time of the Universe, and $\tau_{i,\mathrm{dec}}$ is the decoupling time of the i-particles, defined by the condition $t_i(\tau_{i,\mathrm{dec}}) \sim H^{-1}(\tau_{i,\mathrm{dec}})$ with H being the cosmic expansion rate. As demonstrated in Eq. (2.2), particles no longer contribute to the η once they decouple, and the η is primarily governed by the weakest-interacting particles (with the largest t_i) within the cosmic fluid. Therefore, we can mainly consider the contributions of photons γ, neutrinos ν and some possible weakly-interacting particles beyond the Standard Model (BSM), denoted by X, with their respective mean free times as follows

$$t_\gamma = (n_{e^\pm}\langle\sigma_{\mathrm{KN}}v\rangle)^{-1} , \ t_\nu = (n_\nu\langle\sigma_\nu v\rangle)^{-1} , \ \text{and} \ t_X = (n_X\langle\sigma_X v\rangle)^{-1} . \tag{2.3}$$

In Eq. (2.3), n_i is the number density and $\langle\sigma_i v\rangle$ is the thermally-averaged cross section for the corresponding interactions, i.e., $\langle\sigma_{\mathrm{KN}}v\rangle$ is the Klein-Nishina cross section for photon-electron scattering, $\langle\sigma_\nu v\rangle$ is the weak interaction cross section for neutrinos, and $\langle\sigma_X v\rangle$ is a model-dependent cross section given by the related new physics.

For the interest of GW observations, we focus on the dissipative effects above $\sim$ keV. In this case, the dissipation from photons is negligible [23], and the η is dominated by neutrinos and possible X-particles. At the temperature T, the related quantities of particle species

$j = \{\nu, X\}$ in Eq. (2.2) are given by $\rho_j \sim g_j T^4$, $n_j \sim g_j T^3$ with g_j the degrees of freedom, and $\langle \sigma_j v \rangle$ is generally parameterized at a reference energy scale T_*, i.e.,

$$\langle \sigma_j v \rangle = \langle \sigma_j v \rangle_* \left(\frac{T}{T_*} \right)^{m_j(T)} . \tag{2.4}$$

As an example, we here consider neutrinos within the Standard Model (SM) and new X-particles interacting through the weak interaction mediated by some heavy gauge bosons W'. Then Eq. (2.4) can be specifically expressed as

$$\langle \sigma_\nu v \rangle \simeq \begin{cases} \alpha_F^2/T^2 \,, \ T \gg M_W \,, \\ G_F^2 \, T^2 \,, \ T \lesssim M_W \,, \end{cases} \text{and } \langle \sigma_X v \rangle \simeq \begin{cases} (\alpha')^2/T^2 \,, \ T \gg M_{W'} \,, \\ (G')^2 \, T^2 \,, \ T \lesssim M_{W'} \,. \end{cases} \tag{2.5}$$

Here, $M_W \sim 100\,\mathrm{GeV}$ is the W mass, $G_F \sim 10^{-5}\,\mathrm{GeV}^{-2}$ is the Fermi constant, and $G_F = \alpha_F/M_W^2$. Similarly, $M_{W'}$ is the W' mass with $M_{W'} > M_W$, and we have $G' = G_F(M_W/M_{W'})^2$ and $G' = \alpha'/M_{W'}^2$. The different temperature dependence of $\langle \sigma_j v \rangle$ before and after the phase transitions stems from the fact that the corresponding mediated bosons are massless and massive, respectively. With these particle interactions in the early Universe, we can determine the dissipation in cosmic fluid through Eq. (2.2).

2.2 Evolution of cosmological scalar perturbations

From now, let us move on to the effects of dissipation on cosmological perturbations. In this paper, we adopt a perturbed Friedmann-Robertson-Walker metric in the conformal Newtonian gauge with the anisotropic stress being neglected, i.e.,

$$\mathrm{d}s^2 = a^2(\tau) \left\{ -(1 + 2\phi)\,\mathrm{d}\tau^2 + \left[(1 - 2\phi)\delta_{ij} + \frac{1}{2}h_{ij} \right] \mathrm{d}x^i \mathrm{d}x^j \right\} , \tag{2.6}$$

where a is the scale factor of the Universe, ϕ is the linear scalar perturbations, and h_{ij} is the secondary transverse-traceless tensor perturbations sourced by ϕ, known as IGWs.

Dissipation in cosmic fluid can significantly affect the evolution of ϕ inside the horizon. We define the transfer function $\Phi(k, \tau)$ to describe the evolution of $\phi_{\mathbf{k}}$, i.e.,

$$\phi_{\mathbf{k}}(\tau) = \frac{3 + 3w}{5 + 3w} \, \Phi(k, \tau) \, \zeta_{\mathbf{k}} , \tag{2.7}$$

where $w = p/\rho$ is the parameter of the equation of state, with $w = 1/3$ in the RD era, $\zeta_{\mathbf{k}}$ is primordial curvature perturbations, and $\mathbf{k}$ denotes the Fourier mode of perturbations. Given $\nabla^2 \phi \sim \delta\rho/\rho$, the damping of $\delta\rho$ in the presence of dissipation naturally leads to the damping of ϕ, with their transfer function given by [25]

$$\Phi(k, \tau) \simeq \frac{9}{(k\tau)^2} \left(\frac{\sqrt{3}}{k\tau} \sin\frac{k\tau}{\sqrt{3}} - \cos\frac{k\tau}{\sqrt{3}} \right) e^{-k^2/k_D^2(\tau)} , \tag{2.8}$$

where k_D is a typical damping scale. For the scales $k \ll k_D$, Eq. (2.8) goes back to the standard result in the RD era. While for the small scales $k \gg k_D$, the exponential damping
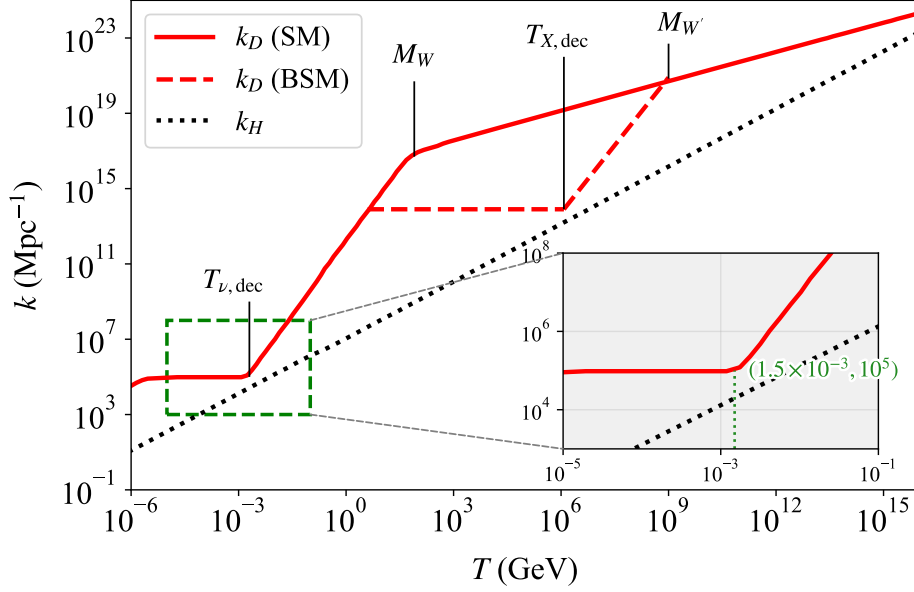
Figure 1. Temperature dependence of the damping scale k_D. Red solid line stands for the SM [25], while red dashed lines denote BSM. We plot the comoving Hubble horizon $k_{\mathcal{H}} = aH$ for comparison.

factor greatly accelerates the decay of $\Phi(k, \tau)$, implying that dissipative effects dominates the evolution of ϕ. The parameter k_D plays the central role in the following discussion. In the early Universe, k_D can be determined by the shear viscosity in cosmic fluid, i.e., [23]

$$k_D^{-2} \simeq \int_0^\tau \mathrm{d}\bar{\tau} \; \frac{2\eta}{3a\,(\rho + p)} \simeq \int_\infty^T \mathrm{d}\bar{T} \left(-\frac{1}{aH\bar{T}} \right) \frac{2\eta}{3a\,(\rho + p)} \;, \tag{2.9}$$

with η given by Eq. (2.2). In the second step, we transform the integral variable from τ to T by using the relation $H \sim T^2/M_{\mathrm{pl}} \sim 2/t$ and $\mathrm{d}\tau/\mathrm{d}T = (1/a)\,\mathrm{d}t/\mathrm{d}T \sim -1/(aHT)$, where M_{pl} is the reduced Planck mass and t is the cosmic physical time.

In Fig. 1, we plot the temperature dependence of k_D above $\sim$ keV. Within the SM, k_D is dominated by neutrino interactions. Using Eqs. (2.2-2.5, 2.9) and neglecting the temperature dependence of the degrees of freedom in cosmic fluid, we have $k_D \propto T^{1/2}$ at $T \gtrsim M_W$, and $k_D \propto T^{5/2}$ at $T \lesssim M_W$. After neutrinos decouple at $T \simeq 1.5\,\mathrm{MeV}$, k_D remains roughly constant at $\sim 10^5\,\mathrm{Mpc}^{-1}$, until the photon interactions start to govern k_D at $\sim$ keV. Additionally, we also consider the case that k_D is dominated by new X-particles with the interactions described by Eq. (2.5). It is straightforward to see that k_D follows the temperature behavior similar to the neutrino-domination case but happens at higher energy scales. In general, the damping of ϕ caused by any new particles can be analyzed by substituting their cross sections into Eqs. (2.2, 2.9).

The evolution of $\phi_{\mathbf{k}}$ inside the horizon depends on the ratio between k_D and the horizon scale $k_{\mathcal{H}} = \mathcal{H} = aH$, where $\mathcal{H}$ is the comoving Hubble parameter. As illustrated in Fig. 1, k_D is usually much larger than $k_{\mathcal{H}}$ but approaches $k_{\mathcal{H}}$ near the decoupling time of

weakly-interacting particles. The latter can be briefly derived as follows. Assuming that η is dominated by the interaction of j-particles given by Eq. (2.4) with $T_* = T_{j,\text{dec}}$ and m_j a constant, k_D at the decoupling of j-particles can be estimated as

$$k_{D,j}^{-2} \simeq \int_\infty^{T_{j,\text{dec}}} \mathrm{d}T \left(-\frac{1}{aHT} \right) \frac{2\,\rho_j t_j}{15\,a\rho} \simeq \frac{1}{m_j + 3} \times \frac{2\,\rho_j t_j}{15\,a^2 H\rho} \bigg|_{T=T_{j,\text{dec}}} \simeq \frac{2\rho_j}{15(m_j + 3)\rho} k_{\mathcal{H},j}^{-2} \,, \tag{2.10}$$

where we introduce $k_{D,j} = k_D(\tau_{j,\text{dec}})$ and $k_{\mathcal{H},j} = k_{\mathcal{H}}(\tau_{j,\text{dec}})$ as short-hand notations. To evaluate the integral above, we should notice that the integrand scales as $\sim T^{-(m_j + 4)}$ and also apply the decoupling condition $t_j \sim H^{-1}$. Eq. (2.10) tells us the important relation

$$\frac{k_{D,j}}{k_{\mathcal{H},j}} \simeq \sqrt{\frac{15(m_j + 3)\rho}{2\rho_j}} \,. \tag{2.11}$$

Note that though we neglect the change of degrees of freedom for simplicity, it is expected to modify the result only by an $\mathcal{O}(1)$ factor. Eq. (2.11) generally implies that $k_{D,j}$ is comparable to $k_{\mathcal{H},j}$ as long as the abundance of j-particles is non-negligible at decoupling. Therefore, the evolution of $\phi_{\mathbf{k}}$ can be concluded as: the modes $k \sim k_{D,j}$ would undergo exponential decay soon after horizon reentry, while for other modes, the damping effects are negligible unless they are deep in the horizon. This also aligns with the physical picture that particle interactions become weakest right before decoupling and cause the maximal dissipation.

In the subsequent discussion, instead of concentrating on specific particle species, we extract the main feature of k_D and utilize a parameterization method to study dissipative effects. Here, we rewrite Eq. (2.8) as the function of dimensionless variables $\kappa = k/k_{\mathcal{H},j} = k\tau_{j,\text{dec}}$ and $\hat{\tau} = \tau/\tau_{j,\text{dec}}$, i.e.,

$$\Phi(\kappa, \hat{\tau}) \simeq \frac{9}{(\kappa\hat{\tau})^2} \left(\frac{\sqrt{3}}{\kappa\hat{\tau}} \sin\frac{\kappa\hat{\tau}}{\sqrt{3}} - \cos\frac{\kappa\hat{\tau}}{\sqrt{3}} \right) e^{-\kappa^2/\kappa_D^2(\hat{\tau})} \,, \tag{2.12}$$

where the reduced damping scale is defined as $\kappa_D(\hat{\tau}) = k_D(\tau)/k_{\mathcal{H},j}$. Based on the discussion in last paragraph, we can focus on the damping effects near the decoupling time of j-particles, and κ_D can be parameterized as

$$\kappa_D(\hat{\tau}) \simeq \begin{cases} \gamma^{-1}\,\hat{\tau}^{-\alpha/2} \,, & \hat{\tau} < 1 \\ \gamma^{-1} \,, & \hat{\tau} > 1 \,. \end{cases} \tag{2.13}$$

The two dissipation parameters α and γ in Eq. (2.13) are defined as

$$\hat{\tau}^{-\alpha/2} \equiv \frac{k_D(\tau)}{k_{D,j}} \simeq \hat{\tau}^{-(m_j+3)/2} \,, \text{ and } \gamma^{-1} \equiv \frac{k_{D,j}}{k_{\mathcal{H},j}} \simeq \sqrt{\frac{15(m_j + 3)\rho}{2\rho_j}} \,, \tag{2.14}$$

respectively. Fig. 2 clearly shows how α and γ determine the evolution of κ_D near the j-particle decoupling. In what follows, we will use α and γ as free parameters to characterize the properties of $\kappa_D(\hat{\tau})$, and they can be connected to the particle interaction and abundance through Eq. (2.14).
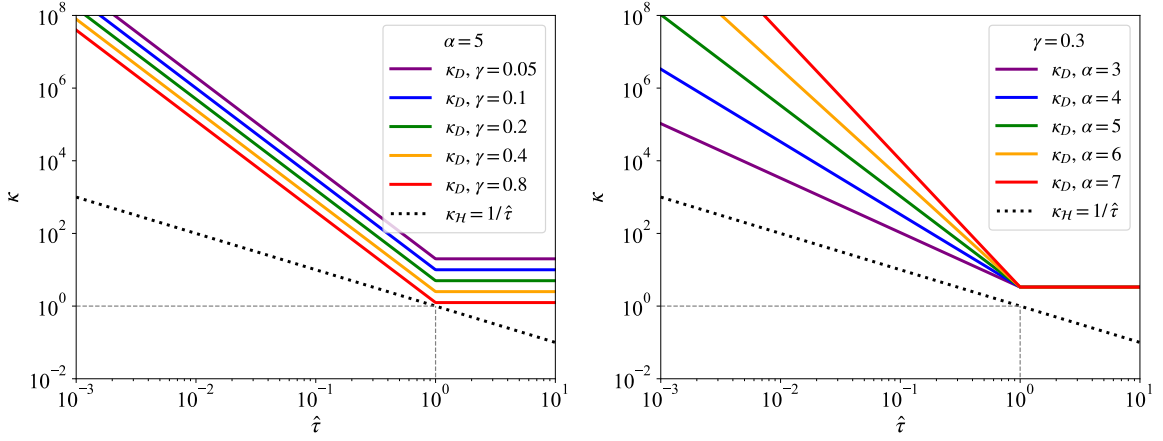
Figure 2. Damping scale κ_D as a function of $\hat{\tau}$ near the particle decoupling for different values of α and γ. The comoving Hubble parameter $\kappa_{\mathcal{H}} = 1/\hat{\tau}$ is also plotted.

2.3 Energy-density spectrum of induced gravitational waves

The preparations in the previous two subsections allow us to further investigate dissipative effects in IGWs. In Eq. (2.6), the IGWs, h_{ij}, can be transformed into Fourier space as

$$h_{ij}(\tau, \mathbf{x}) = \sum_{\lambda=+,\times} \int \frac{\mathrm{d}^3 \mathbf{k}}{(2\pi)^{3/2}} \, e^{i\mathbf{k}\cdot\mathbf{x}} \, \epsilon^\lambda_{ij,\mathbf{k}} \, h^\lambda_{\mathbf{k}}(\tau) \, , \tag{2.15}$$

where $\lambda = +, \times$ denotes two polarization modes of GWs, and the two polarization tensors $\epsilon^\lambda_{ij,\mathbf{k}}$ are defined as $\epsilon^+_{ij,\mathbf{k}} = [\epsilon_{i,\mathbf{k}} \epsilon_{j,\mathbf{k}} - \bar{\epsilon}_{i,\mathbf{k}} \bar{\epsilon}_{j,\mathbf{k}}]/\sqrt{2}$ and $\epsilon^\times_{ij,\mathbf{k}} = [\epsilon_{i,\mathbf{k}} \epsilon_{j,\mathbf{k}} + \bar{\epsilon}_{i,\mathbf{k}} \bar{\epsilon}_{j,\mathbf{k}}]/\sqrt{2}$, respectively, with $\epsilon_{i,\mathbf{k}}$ and $\bar{\epsilon}_{i,\mathbf{k}}$ forming an orthonormal basis perpendicular to $\mathbf{k}$. Based on cosmological perturbation theory, the motion of $h^\lambda_{\mathbf{k}}$ satisfies

$$h^{\lambda}_{\mathbf{k}}{}''(\tau) + 2\mathcal{H} h^{\lambda}_{\mathbf{k}}{}'(\tau) + k^2 h^\lambda_{\mathbf{k}}(\tau) = 4 \mathcal{S}^\lambda_{\mathbf{k}}(\tau) \, , \tag{2.16}$$

where a prime stands for a derivative with respect to τ, and the source term reads

$$\mathcal{S}^\lambda_{\mathbf{k}} = \int \frac{\mathrm{d}^3 \mathbf{q}}{(2\pi)^{3/2}} \, \epsilon^\lambda_{ij,\mathbf{k}} \, q_i q_j \times \left[2\phi_{\mathbf{k}-\mathbf{q}}\phi_{\mathbf{q}} + (\mathcal{H}^{-1}\phi'_{\mathbf{k}-\mathbf{q}} + \phi_{\mathbf{k}-\mathbf{q}})(\mathcal{H}^{-1}\phi'_{\mathbf{q}} + \phi_{\mathbf{q}}) \right] \, . \tag{2.17}$$

By employing the Green's function method [18, 19], Eq. (2.16) can be solved as

$$a(\tau)h^\lambda_{\mathbf{k}}(\tau) = 4 \int^\tau \mathrm{d}\tau_1 \, G_{\mathbf{k}}(\tau, \tau_1) \, a(\tau_1) \mathcal{S}^\lambda_{\mathbf{k}}(\tau_1) \, . \tag{2.18}$$

Here, $G_{\mathbf{k}}(\tau, \tau_1)$ stands for the Green's function, which is defined as the solution of the Green's equation

$$G''_{\mathbf{k}}(\tau, \tau_1) + \left(k^2 - \frac{a''(\tau)}{a(\tau)} \right) G_{\mathbf{k}}(\tau, \tau_1) = \delta(\tau - \tau_1) \, , \tag{2.19}$$

and the expression of $G_{\mathbf{k}}(\tau, \tau_1)$ is obtained to be

$$G_{\mathbf{k}}(\tau, \tau_1) = \sin(k\tau - k\tau_1)/k \, . \tag{2.20}$$

To relate IGWs with ζ, we rewrite Eqs. (2.17, 2.18) in the form of

$$h_{\mathbf{k}}^{\lambda}(\tau) = 4 \int \frac{\mathrm{d}^3 \mathbf{q}}{(2\pi)^{3/2}} \, Q^{\lambda}(\mathbf{k}, \mathbf{q}) \, I(|\mathbf{k} - \mathbf{q}|, q, \tau) \, \zeta_{\mathbf{k}-\mathbf{q}} \, \zeta_{\mathbf{q}} \, . \tag{2.21}$$

Here, the projection factor $Q^{\lambda}(\mathbf{k}, \mathbf{q})$ describes the geometric relations between the momenta and polarization tensors of the linear perturbations, being defined as

$$Q^{\lambda}(\mathbf{k}, \mathbf{q}) = \epsilon_{ij,\mathbf{k}}^{\lambda} \, q_i q_j / \, k^2 \tag{2.22}$$

and the kernel function $I(|\mathbf{k} - \mathbf{q}|, q, \tau)$ encodes the evolution information of GW sources after inflation, which is given by

$$I(|\mathbf{k} - \mathbf{q}|, q, \tau) = \int_0^{k\tau} \mathrm{d}(k\tau_1) \, \frac{a(\tau_1)}{a(\tau)} \, k G_{\mathbf{k}}(\tau, \tau_1) \, f(|\mathbf{k} - \mathbf{q}|, q, \tau_1) \, . \tag{2.23}$$

where $f(|\mathbf{k} - \mathbf{q}|, q, \tau)$ is constructed from the combination of transfer functions in Eq. (2.8), i.e.,

$$\begin{aligned} f(|\mathbf{k} - \mathbf{q}|, q, \tau_1) = \; & \frac{4}{3} \, \Phi(|\mathbf{k} - \mathbf{q}|, \tau_1) \, \Phi(q, \tau_1) + \frac{4}{9} \, \tau_1^2 \, \Phi'(|\mathbf{k} - \mathbf{q}|, \tau_1) \, \Phi'(q, \tau_1) \\ & + \frac{4}{9} \left[\tau_1 \, \Phi(|\mathbf{k} - \mathbf{q}|, \tau_1) \, \Phi'(q, \tau_1) + \tau_1 \, \Phi'(|\mathbf{k} - \mathbf{q}|, \tau_1) \, \Phi(q, \tau_1) \right] \, . \end{aligned} \tag{2.24}$$

Here, we remind that Φ is dependent on dissipation parameters α and γ, and dissipative effects enter into IGWs through the exponential damping of GW sources.

The IGWs naturally form a stochastic background in the early Universe. As the most basic observable to describe its statistical properties, the energy-density fraction spectrum of IGWs, $\Omega_{\mathrm{gw}}(k)$, defined as the GW energy density ρ_{gw} per logarithmic wavenumber normalized by the Universe's critical energy density ρ_{c}, can be calculated as follows

$$\Omega_{\mathrm{gw}}(k) = \frac{1}{\rho_c} \frac{\mathrm{d}\,\rho_{\mathrm{gw}}}{\mathrm{d}\ln k} = \frac{1}{48} \left(\frac{k}{\mathcal{H}} \right)^2 \sum_{\lambda = +, \times} \mathcal{P}_h^{\lambda}(k) \, , \tag{2.25}$$

where $\mathcal{P}_h^{\lambda}(k)$ is the dimensionless power spectrum of IGWs, which is defined by the two-point correlation of $h_{\mathbf{k}}^{\lambda}$, i.e.,

$$\langle h_{\mathbf{k}}^{\lambda} \, h_{\mathbf{k}'}^{\lambda'} \rangle = \delta^{\lambda\lambda'} \, \delta^{(3)}(\mathbf{k} + \mathbf{k}') \, \frac{2\pi^2}{k^3} \, \mathcal{P}_h^{\lambda}(k) \, . \tag{2.26}$$

Eqs. (2.21, 2.25, 2.26) indicate $\Omega_{\mathrm{gw}} \sim \langle h^2 \rangle \sim \langle \mathcal{S}^{\lambda}(\tau_1) \mathcal{S}^{\lambda}(\tau_2) \rangle \propto \langle \zeta^4 \rangle$. With the assumption of the Gaussianity of ζ, the four-point correlator $\langle \zeta^4 \rangle$ factorizes into products of $\langle \zeta^2 \rangle$ through Wick's theorem, expressed in terms of the primordial curvature power spectrum $\mathcal{P}_{\zeta}$, which is defined by

$$\langle \zeta_{\mathbf{k}} \, \zeta_{\mathbf{k}'} \rangle = \delta^{(3)}(\mathbf{k} + \mathbf{k}') \, \frac{2\pi^2}{k^3} \, \mathcal{P}_{\zeta}(k) \, . \tag{2.27}$$

For a parametric treatment of dissipative effects in IGWs, it is convenient to work with dimensionless variables, i.e., $u = |\mathbf{k} - \mathbf{q}|/k$, $v = q/k$, along with κ and $\hat{\tau}$ introduced previously. After straightforward calculations, Ω_{gw} can be obtained as [18, 19]

$$\Omega_{\mathrm{gw}}(\kappa, \hat{\tau}) = \frac{1}{6} \int_0^{\infty} \mathrm{d}u \int_{|1-u|}^{1+u} \mathrm{d}v \, Q^2(u, v) \, \overline{\mathcal{I}^2(u, v, \kappa, \hat{\tau})} \times \mathcal{P}_{\zeta}(u\kappa) \mathcal{P}_{\zeta}(v\kappa) \, . \tag{2.28}$$

In Eq. (2.28), the geometric factor $Q^2(u, v)$ is given by

$$Q^2(u, v) = \delta^{\lambda\lambda'} Q^\lambda(\mathbf{k}, \mathbf{q}) \, Q^{\lambda'}(\mathbf{k}, \mathbf{q}) = \left[\frac{4v^2 - (1 + v^2 - u^2)^2}{4uv} \right]^2 , \qquad (2.29)$$

and $\mathcal{I}(u, v, \kappa, \hat{\tau})$ is defined by $(k/\mathcal{H}) \, I(|\mathbf{k} - \mathbf{q}|, q, \tau)$, with the oscillation average of $\mathcal{I}^2(u, v, \kappa, \hat{\tau})$ given by

$$\overline{\mathcal{I}^2(u, v, \kappa, \hat{\tau})} = \int_0^{\kappa\hat{\tau}} \mathrm{d}(\kappa\hat{\tau}_1) \int_0^{\kappa\hat{\tau}} \mathrm{d}(\kappa\hat{\tau}_2) \times \frac{1}{2} \left\{ \prod_{i=1,2} \left[\kappa\hat{\tau}_i \, \cos(\kappa\hat{\tau}_i) \, f(u\kappa, v\kappa, \hat{\tau}_i) \right] \right.$$
$$\left. + \prod_{i=1,2} \left[\kappa\hat{\tau}_i \, \sin(\kappa\hat{\tau}_i) \, f(u\kappa, v\kappa, \hat{\tau}_i) \right] \right\} , \qquad (2.30)$$

Here, $f(u\kappa, v\kappa, \hat{\tau}_i)$ is derived from Eq. (2.24) by substituting $|\mathbf{k} - \mathbf{q}| \to u\kappa$, $q \to v\kappa$ and $\tau_i \to \hat{\tau}_i$, and $\Phi(\kappa, \hat{\tau})$ is given by Eqs. (2.12, 2.13).

With Eqs. (2.28, 2.30), we can calculate the IGW spectrum. In the dissipation-free case, i.e., $\kappa_D \to \infty$, $\mathcal{I}(u, v, \kappa, \hat{\tau})$ has an analytical expression, namely [19]

$$\mathcal{I}(u, v, \kappa, \hat{\tau}) = \frac{9}{u^3 v^3 (\kappa\hat{\tau})^3} \left\{ 2uv(\kappa\hat{\tau})^2 \cos\frac{u\kappa\hat{\tau}}{\sqrt{3}} \cos\frac{v\kappa\hat{\tau}}{\sqrt{3}} - 2\sqrt{3}\, u(\kappa\hat{\tau}) \cos\frac{u\kappa\hat{\tau}}{\sqrt{3}} \sin\frac{v\kappa\hat{\tau}}{\sqrt{3}} \right.$$

$$\left. - 2\sqrt{3}\, v(\kappa\hat{\tau}) \sin\frac{u\kappa\hat{\tau}}{\sqrt{3}} \cos\frac{v\kappa\hat{\tau}}{\sqrt{3}} + \left[6 + (u^2 + v^2 - 3)(\kappa\hat{\tau})^2 \right] \sin\frac{u\kappa\hat{\tau}}{\sqrt{3}} \sin\frac{v\kappa\hat{\tau}}{\sqrt{3}} \right\}$$

$$+ \frac{3(u^2 + v^2 - 3)\sin(\kappa\hat{\tau})}{4u^3 v^3} \left\{ (u^2 + v^2 - 3) \left[\mathrm{Ci}\left(\left(1 - \frac{v-u}{\sqrt{3}} \right) \kappa\hat{\tau} \right) + \mathrm{Ci}\left(\left(1 + \frac{v-u}{\sqrt{3}} \right) \kappa\hat{\tau} \right) \right. \right.$$

$$\left. \left. - \mathrm{Ci}\left(\left| 1 - \frac{v+u}{\sqrt{3}} \right| \kappa\hat{\tau} \right) - \mathrm{Ci}\left(\left(1 + \frac{v+u}{\sqrt{3}} \right) \kappa\hat{\tau} \right) + \ln\left(\left| \frac{3 - (u+v)^2}{3 - (u-v)^2} \right| \right) \right] - 4uv \right\}$$

$$- \frac{3(u^2 + v^2 - 3)\cos(\kappa\hat{\tau})}{4u^3 v^3} \left\{ (u^2 + v^2 - 3) \left[\mathrm{Si}\left(\left(1 - \frac{v-u}{\sqrt{3}} \right) \kappa\hat{\tau} \right) + \mathrm{Si}\left(\left(1 + \frac{v-u}{\sqrt{3}} \right) \kappa\hat{\tau} \right) \right. \right.$$

$$\left. \left. - \mathrm{Si}\left(\left(1 - \frac{v+u}{\sqrt{3}} \right) \kappa\hat{\tau} \right) - \mathrm{Si}\left(\left(1 + \frac{v+u}{\sqrt{3}} \right) \kappa\hat{\tau} \right) \right] \right\} . \qquad (2.31)$$

In Eq. (2.31), the sine/cosine-integral and logarithmic functions come from the relations

$$\int_0^x \mathrm{d}\bar{x} \, \frac{\sin A\bar{x}}{\bar{x}} = \mathrm{Si}(Ax) , \quad \text{and} \quad \int_0^x \mathrm{d}\bar{x} \, \frac{1 - \cos A\bar{x}}{\bar{x}} = \gamma_E - \mathrm{Ci}(|Ax|) + \ln|Ax| , \qquad (2.32)$$

where $\gamma_E \simeq 0.577$ is the Euler-Mascheroni constant. Taking the late-time limit, i.e., $\kappa\hat{\tau} \to \infty$, Eq. (2.31) can be derived to the simple form

$$\mathcal{I} = \frac{3(u^2 + v^2 - 3)^2}{4u^3 v^3} \left[\left(\ln\left| \frac{3 - (u+v)^2}{3 - (u-v)^2} \right| - \frac{4uv}{u^2 + v^2 - 3} \right) \sin(\kappa\hat{\tau}) - \pi\,\Theta(u + v - \sqrt{3}) \cos(\kappa\hat{\tau}) \right] , \qquad (2.33)$$

which avoids the highly-oscillating time integral in Eq. (2.30) and largely simplifies the calculation of $\Omega_{\mathrm{gw}}(\kappa)$. However, given κ_D in Eq. (2.13), $\mathcal{I}(u, v, \kappa, \hat{\tau})$ generally lacks any analytical

expressions. We numerically calculate the $\Omega_{\rm gw}$ using an open Python package `vegas` [29] [1], as will be shown in Section 3.

Before ending this section, we provide an intuitive physical picture about how dissipation affects the IGW production. Particularly, we introduce the conception of "dissipation-induced lifetime" of GW sources, which is crucial for subsequent analysis. This conception is based on the following facts. Without dissipation, $\phi_{\bf k}$ decays only slowly inside the horizon, roughly as $\sim 1/(\kappa\hat\tau)^2$, remaining an active GW source until $\kappa\hat\tau \gg 1$. However, with dissipation, the additional damping factor $\sim e^{-\kappa^2/\kappa_D^2(\hat\tau)}$ can significantly accelerate the decay of $\phi_{\bf k}$ for the mode $\kappa > \kappa_D(\hat\tau)$. When only a rough analysis is conducted, we can simply assume that dissipation effects can be ignored before $\kappa \sim \kappa_D(\hat\tau)$, while that GW sources immediately vanish after $\kappa \sim \kappa_D(\hat\tau)$. Mathematically, this is equivalent to making the following approximation in Eq. (2.12)

$$e^{-\kappa^2/\kappa_D^2(\hat\tau)} \sim \Theta(\hat\tau_l - \hat\tau) \ , \quad \text{where } \kappa \sim \kappa_D(\hat\tau_l) \ . \tag{2.34}$$

Here, we refer $\hat\tau_l$ to as the "dissipation-induced lifetime" of $\phi_{\bf k}$, which is determined by the mode κ as well as the dissipation parameters α and γ. The IGWs could only be efficiently produced within the lifetimes of sources. This approximation enables us to make use of the analytical results in Eq. (2.31) and will largely simplify our analysis.

3 Dissipative effects in the induced gravitational waves

Based on the foundation established in Section 2, we present the numerical results of $\Omega_{\rm gw}$ in the presence of dissipation for different types of $\mathcal{P}_\zeta$ (i.e., scale-invariant, monochromatic, and log-normal ones). For each $\mathcal{P}_\zeta$, we study the dependence of dissipative effects in $\Omega_{\rm gw}$ on the dissipation parameters α and γ. Furthermore, we also reveal the physical origins behind these results, which are critical for us to link GW observables to the early Universe. We summarize the basic properties of dissipative effects in IGWs at the end of this section.

3.1 Scale-invariant curvature power spectrum

Firstly, let us consider the simplest case where ζ has a scale-invariant spectrum

$$\mathcal{P}_\zeta(\kappa) = \mathcal{A}_\zeta \ , \tag{3.1}$$

where $\mathcal{A}_\zeta$ is a spectral amplitude. This model can be an approximation of those flat spectra within the relevant range of scales. In the dissipation-free limit $\kappa_D \to \infty$, the corresponding IGW spectrum is given by

$$\Omega_{\rm gw}^{\kappa_D \to \infty}(\kappa) = 0.822\, \mathcal{A}_\zeta^2 \ . \tag{3.2}$$

---

[1]In the numerical integral in Eq. (2.30), the choice of the upper limit $\kappa\hat\tau$ should balance the following two aspects. On the one hand, $\kappa\hat\tau$ should be sufficiently large to ensure the late-time limit. The production of IGWs is almost completed before this $\kappa\hat\tau$ and $\Omega_{\rm gw}(\kappa)$ remains constant with the further increase of $\kappa\hat\tau$. On the other hand, for a too much large $\kappa\hat\tau$, the finite number of scattering points in the domain of integration may not accurately describe the highly oscillating integrand function, thus resulting in the distortion of numerical integral results.
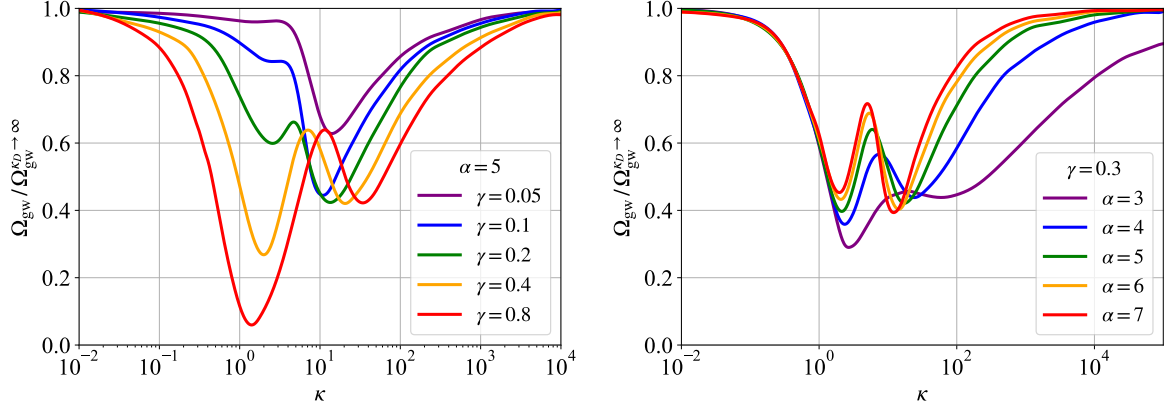
Figure 3. Energy-density spectrum Ω_{gw} (normalized by $\Omega_{\text{gw}}^{\kappa_D \to \infty} = 0.822\,\mathcal{A}_\zeta^2$) versus the scale κ for scale-invariant primordial curvature power spectra. In the left panel, we fix $\alpha = 5$ and take $\gamma = 0.05, 0.1, 0.2, 0.4, 0.8$. In the right panel, we fix $\gamma = 0.3$ and take $\alpha = 3, 4, 5, 6, 7$.

Since $\Omega_{\text{gw}}^{\kappa_D \to \infty}$ is also scale-invariant, all the possible features in Ω_{gw} could only come from dissipative effects, serving as an appropriate example to study them.

In Fig. 3, we present the IGW spectra with different dissipative parameters γ and α in the left and right panel, respectively. As shown in both panels, dissipative effects generally introduce multi(double) valleys, whose positions and shapes are dependent on γ and α. The left valley locates at $\kappa \sim \mathcal{O}(1)$ with its position remaining relatively stable across the γ and α range. It becomes deeper as γ increases and α decreases, and, particularly, can vanish for a sufficiently small γ. The right valley locates at $\kappa \gtrsim \mathcal{O}(10)$, and its position shows a more pronounced sensitivity, shifting towards larger κ for increasing γ and decreasing α. Meanwhile, larger γ and smaller α values tend to broaden the right valley, but its depth seems less sensitively dependent on these parameters. For $\kappa \ll 1$ and $\kappa \to \infty$, the GW spectrum goes back to the result without dissipation, implying that the dissipative effects become not important at the scales far away from the damping scale $k_{D,j}$.

These features in Ω_{gw} for a scale-invariant $\mathcal{P}_\zeta$ arise from the oscillating properties of GW sources during their dissipation-induced lifetimes. To better understand this, we recast Eqs. (2.28, 2.30) into the form

$$\Omega_{\text{gw}}(\kappa, \tau) = \int_0^{\kappa\hat{\tau}} \mathrm{d}(\kappa\hat{\tau}_1) \int_0^{\kappa\hat{\tau}} \mathrm{d}(\kappa\hat{\tau}_2) \left[\int_0^\infty \mathrm{d}u \int_{|1-u|}^{1+u} \mathrm{d}v \; \omega_{\text{gw}}(u, v, \kappa, \hat{\tau}_1, \hat{\tau}_2) \right], \qquad (3.3)$$

where [...] is the "Green function" contacting Ω_{gw} to GW sources at any given time $(\hat{\tau}_1, \hat{\tau}_2)$, with $\omega_{\text{gw}}(u, v, \kappa, \hat{\tau}_1, \hat{\tau}_2)$ a combination of geometric factor, transfer functions, and primordial

curvature power spectra, i.e.,

$$\omega_{\text{gw}}(u, v, \kappa, \hat{\tau}_1, \hat{\tau}_2) = \frac{1}{12} Q^2(u, v) \left\{ \prod_{i=1,2} \left[\kappa\hat{\tau}_i \cos\left(\kappa\hat{\tau}_i\right) f(u\kappa, v\kappa, \hat{\tau}_i) \right] \right. $$
$$\left. + \prod_{i=1,2} \left[\kappa\hat{\tau}_i \sin\left(\kappa\hat{\tau}_i\right) f(u\kappa, v\kappa, \hat{\tau}_i) \right] \right\} \mathcal{P}_\zeta(u\kappa)\mathcal{P}_\zeta(v\kappa) \, . \tag{3.4}$$

Based on the approximation in Eq. (2.34), within the lifetimes of GW sources, Eq. (3.4) can be treated the same as the dissipation-free case. Since [...] in Eq. (3.3) is mainly contributed from $u, v \sim 1$ for scale-invariant $\mathcal{P}_\zeta$, we consider the properties of $\omega_{\text{gw}}^{\kappa_D \to \infty}(1, 1, \kappa, \hat{\tau}_1, \hat{\tau}_2)$, which is plotted as a function of $\kappa\tau_1$ and $\kappa\tau_2$ in Fig. 4. Consisting of products of triangle functions, it oscillates in the $(\kappa\hat{\tau}_1, \kappa\hat{\tau}_2)$ plane, with red and blue regions representing the positive and negative contribution to IGW spectrum, respectively. To obtain the Ω_{gw} in the presence of dissipation, the time integral of $\Omega_{\text{gw}}(\kappa)$ in Eq. (3.3) can be effectively limited in the region of $(0 < \kappa\hat{\tau}_1 < \kappa\hat{\tau}_l, \ 0 < \kappa\hat{\tau}_2 < \kappa\hat{\tau}_l)$. Due to the κ-dependence of τ_l in Eq. (2.34), this integral region varies with different scales. Therefore, the oscillating phase of $\omega_{\text{gw}}^{\kappa_D \to \infty}(1, 1, \kappa, \hat{\tau}_1, \hat{\tau}_2)$ within the integral region could naturally induce peaks/valleys in $\Omega_{\text{gw}}(\kappa)$. Meanwhile, since $\hat{\tau}_l$ also depends on α and γ, the locations and shapes of these peaks/valleys would change with these dissipation parameters.

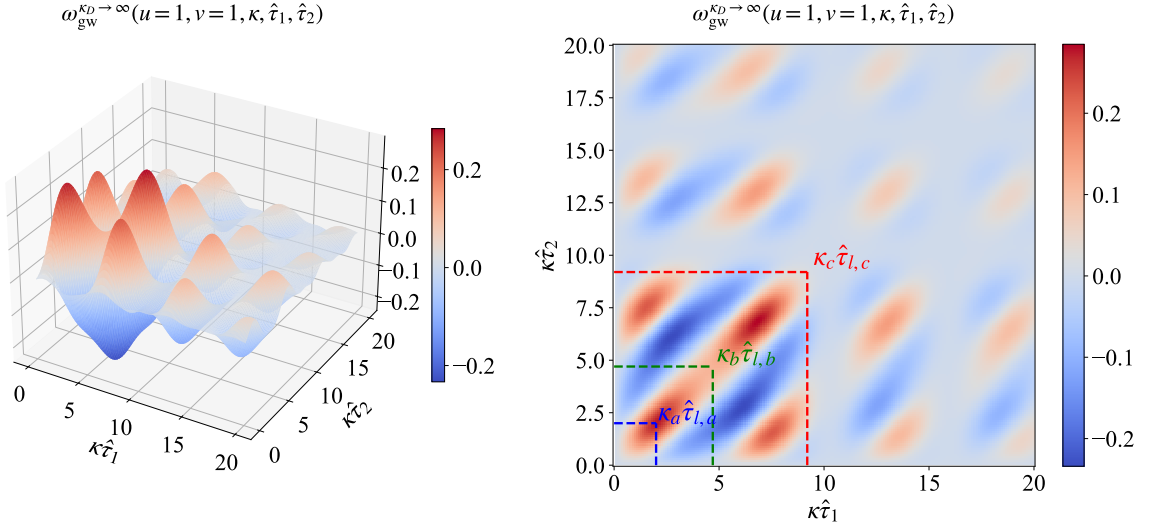**Figure 4**. The 3D graph and heat map of $\omega_{\text{gw}}^{\kappa_D \to \infty}(1, 1, \kappa, \hat{\tau}_1, \hat{\tau}_2)$ as a function of $\kappa\hat{\tau}_1$ and $\kappa\hat{\tau}_2$. The red and blue regions correspond to the positive and negative values, respectively. In the right panel, we mark the integral regions given by the "dissipation-induced lifetimes" of the modes $\kappa_a = 2$ (blue dashed lines), $\kappa_b = 6$ (green dashed lines), and $\kappa_c = 18$ (red dashed lines).

Let us demonstrate in detail how the features in Ω_{gw} are induced by dissipation in a specific example. In the left panel of Fig. 5, we plot $\Omega_{\text{gw}}(\kappa)$ with $\alpha = 5$ and $\gamma = 0.3$, and mark several reference scales (i.e., $\kappa_a = 2$, $\kappa_b = 6$, and $\kappa_c = 18$), which roughly correspond to the locations of valleys/peaks in Ω_{gw}. According to Eq. (2.34), the dissipation-induced lifetimes of

these modes are respectively given by $\kappa_a \hat{\tau}_{l,a} = 2.0$, $\kappa_b \hat{\tau}_{l,b} = 4.7$, and $\kappa_c \hat{\tau}_{l,c} = 9.2$, as signed in the right panel of Fig. 5 [2]. Moreover, the corresponding integral regions ($0 < \kappa \hat{\tau}_1 < \kappa_i \hat{\tau}_{l,i}$, $0 < \kappa \hat{\tau}_2 < \kappa_i \hat{\tau}_{l,i}$) for κ_i ($i = a, b, c$) are also marked in Fig. 4. Based on Fig. 4, the features in $\Omega_{\text{gw}}(\kappa)$ can be derived from the oscillating behavior of $\omega_{\text{gw}}^{\kappa_D \to \infty}$ in the integral regions. (i) For $\kappa \ll 1$ or $\kappa \to \infty$, the integral regions are given by $\kappa \hat{\tau}_l \to \infty$, leading to the same result as the dissipaton-free case. (ii) Since the integral in ($0 < \kappa \hat{\tau}_1 < \kappa_a \hat{\tau}_{l,a}$, $0 < \kappa \hat{\tau}_2 < \kappa_a \hat{\tau}_{l,a}$) is less than that in dissipation-free case, there exhibits a valley in $\Omega_{\text{gw}}(\kappa)$ at $\kappa \sim \kappa_a$. (iii) Since the integral region ($\kappa_a \hat{\tau}_{l,a} < \kappa \hat{\tau}_1 < \kappa_b \hat{\tau}_{l,b}$, $\kappa_a \hat{\tau}_{l,a} < \kappa \hat{\tau}_2 < \kappa_b \hat{\tau}_{l,b}$) is dominated by a positive peak of $\omega_{\text{gw}}^{\kappa_D \to \infty}$, the difference between $\Omega_{\text{gw}}(\kappa_b)$ and $\Omega_{\text{gw}}(\kappa_a)$ is positive. (iv) Since the integral region ($\kappa_b \hat{\tau}_{l,b} < \kappa \hat{\tau}_1 < \kappa_c \hat{\tau}_{l,c}$, $\kappa_b \hat{\tau}_{l,b} < \kappa \hat{\tau}_2 < \kappa_c \hat{\tau}_{l,c}$) is dominated by two negative valleys of $\omega_{\text{gw}}^{\kappa_D \to \infty}$, the difference between $\Omega_{\text{gw}}(\kappa_c)$ and $\Omega_{\text{gw}}(\kappa_b)$ is negative. (v) Similarly, we expect more peaks/valleys on Ω_{gw} for $\kappa \gg \kappa_c$. However, they are not that notable since the oscillations of $\omega_{\text{gw}}^{\kappa_D \to \infty}$ in ($\kappa \hat{\tau}_1 > \kappa_c \hat{\tau}_{l,c}$, $\kappa \hat{\tau}_2 > \kappa_c \hat{\tau}_{l,c}$) are much less pronounced than previous ones.
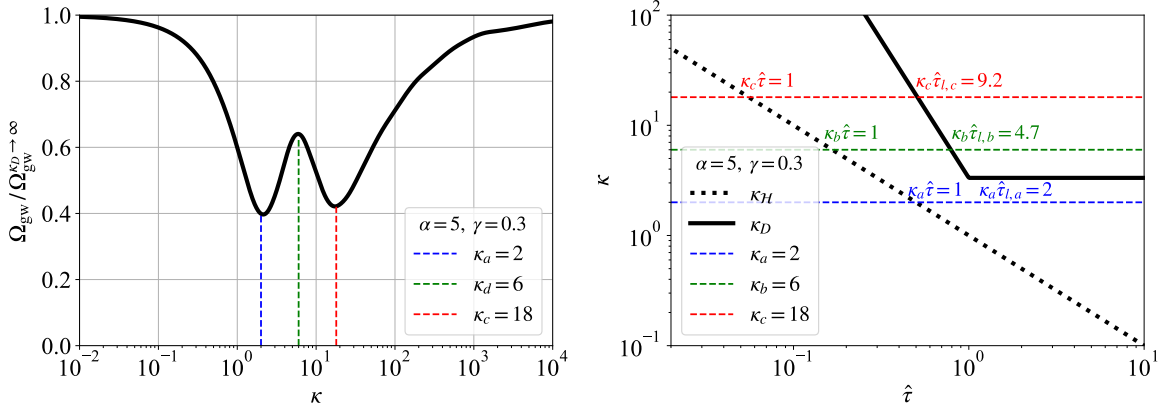

Figure 5. Left panel: Energy-density spectrum Ω_{gw} (normalized by $\Omega_{\text{gw}}^{\kappa_D \to \infty} = 0.822 \mathcal{A}_\zeta^2$) versus the scale κ for scale-invariant primordial curvature power spectra. Right panel: Damping scale κ_D as a function of $\hat{\tau}$ near the particle decoupling. In both panels, we mark the several reference scales (i.e., $\kappa_a = 2$, $\kappa_b = 6$, and $\kappa_c = 18$), which correspond to the positions of peaks/valleys in Ω_{gw}. We set $\alpha = 5$ and $\gamma = 0.3$.

Similar analyses can be applied to general cases. Particularly, we find that even the following simple estimate can decently describe the features on $\Omega_{\text{gw}}(\kappa)$. For $\kappa \hat{\tau}_1, \kappa \hat{\tau}_2 \gg 1$, the oscillating behavior of $\omega_{\text{gw}}^{\kappa_D \to \infty}(1, 1, \kappa, \hat{\tau}_1, \hat{\tau}_2)$ can be roughly described as

$$\omega_{\text{gw}}^{\kappa_D \to \infty}(1, 1, \kappa, \hat{\tau}_1, \hat{\tau}_2) \sim \frac{1 - \cos\left(2\kappa \hat{\tau}_1/\sqrt{3}\right)}{\kappa \hat{\tau}_1} \times \frac{1 - \cos\left(2\kappa \hat{\tau}_2/\sqrt{3}\right)}{\kappa \hat{\tau}_2} \tag{3.5}$$

---

[2]In this example, κ_D can approach κ_a but $\kappa_D(\tau) = \kappa_a$ has no solution. Here, we simply take $\hat{\tau}_{l,a}$ as the initial moment when κ_D is closest to κ_a, namely, $\hat{\tau}_{l,a} = 1$, as an approximation. This treatment will not affect our analysis.

If κ is the location of peaks/valleys, the corresponding integral region ($0 < \kappa\hat{\tau}_1 < \kappa\hat{\tau}_l$, $0 < \kappa\hat{\tau}_2 < \kappa\hat{\tau}_l$) should roughly end at the zero point of Eq. (3.5), i.e.,

$$\kappa\hat{\tau}_l(\kappa,\alpha,\gamma) \simeq \sqrt{3}\,n\pi \ , \ \ n = 1, 2... \ . \tag{3.6}$$

Here, the dissipation-induced lifetime for mode κ can be obtained by substituting $\kappa_D = \gamma^{-1}\hat{\tau}^{-\alpha/2}$ into Eq. (2.34), namely

$$\hat{\tau}_l(\kappa,\alpha,\gamma) = (\gamma\kappa)^{-2/\alpha} \ . \tag{3.7}$$

Combining Eqs. (3.7, 3.6), the locations of peaks/valleys are given by

$$\kappa \simeq (\sqrt{3}\,n\pi)^{\alpha/(\alpha-2)}\gamma^{2/(\alpha-2)} \ , \ \ n = 1, 2... \ . \tag{3.8}$$

In Table 1, we list the locations of the peaks (for $n = 1$) and valleys (for $n = 2$) that predicted by Eq. (3.8), with the same values of α and γ as those in Fig. 3. It can be verified that the results given by Eq. (3.8) approximately consist with the numerical results in Fig. 3. This implies that our estimate captures the main properties of dissipative effects in IGWs.

		$\gamma = 0.05$	$\gamma = 0.1$	$\gamma = 0.2$	$\gamma = 0.4$	$\gamma = 0.8$
$\alpha = 5$	$n = 1$ (peak)	2.3	3.6	5.8	9.1	14.5
	$n = 2$ (valley)	7.3	11.5	18.2	29.0	46.1
		$\alpha = 3$	$\alpha = 4$	$\alpha = 5$	$\alpha = 6$	$\alpha = 7$
$\gamma = 0.3$	$n = 1$ (peak)	14.5	8.9	7.5	7.0	6.6
	$n = 2$ (valley)	116.0	35.5	24.0	19.7	17.5

Table 1. Positions of peaks/valleys on $\Omega_{\text{gw}}(\kappa)$ for different dissipation parameters α and γ, as predicted by Eq. (3.8).

3.2 Monochromatic curvature power spectrum

We then consider another case that ζ has a monochromatic spectrum, which can be modeled by the Dirac function, i.e.,

$$\mathcal{P}_\zeta(\kappa) = \mathcal{A}_\zeta\,\delta\left(\ln\frac{\kappa}{\kappa_\zeta}\right) \ , \tag{3.9}$$

where $\mathcal{A}_\zeta$ is an overall normalized factor and κ_ζ gives the peak wavenumber. This serves as an idealized approximation for a sharply-peaked spectrum. In the dissipation-free limit, the IGW spectrum is given by

$$\begin{aligned}
\Omega_{\text{gw}}^{\kappa_D\to\infty}(\kappa) = \ &\frac{3\mathcal{A}_\zeta^2}{1024}\,\Theta\left(2 - \tilde{\kappa}\right)\tilde{\kappa}^2\left(4 - \tilde{\kappa}^2\right)^2\left(3\tilde{\kappa}^2 - 2\right)^2 \\
&\times\left\{\pi^2\left(3\tilde{\kappa}^2 - 2\right)^2\Theta\left(2\sqrt{3} - 3\tilde{\kappa}\right) + \left[4 + \left(3\tilde{\kappa}^2 - 2\right)\ln\left|\frac{4}{3\tilde{\kappa}^2} - 1\right|\right]^2\right\} \ ,
\end{aligned} \tag{3.10}$$

where $\tilde{\kappa} = \kappa/\kappa_\zeta$. This spectrum is well-known as the following properties: (i) a sharp peak at the logarithmic singularity $\kappa = (2/\sqrt{3})\,\kappa_\zeta$; (ii) a sharp valley near the zero point $\kappa = \sqrt{2/3}\,\kappa_\zeta$; (iii) a logarithmic running $\sim \kappa^2 \ln^2 \kappa$ in the infrared region.

Fig. 6 displays the IGW spectra for a monochromatic $\mathcal{P}_\zeta$ with different choices of dissipation parameters α, γ, and the peak position κ_ζ. Each panel varies one parameter while keeping the other two fixed. Across all panels in our plots, dissipative effects induces several common modifications compared to the spectrum given by Eq. (3.10): (i) The resonant peak at $\kappa = (2/\sqrt{3})\,\kappa_\zeta$ is suppressed and broadened. This suppression becomes more pronounced for larger γ and smaller α, κ_ζ. (ii) The valley near $\kappa = \sqrt{2/3}\,\kappa_\zeta$ is progressively smoothed out. The effect is enhanced by increasing γ and descreasing α, κ_ζ. This valley structure could even disappear under sufficiently strong dissipation. (iii) The infrared region generally transitions from a logarithmic running $\sim \kappa^2 \ln^2 \kappa$ to a steeper scaling $\sim \kappa^2$, indicating stronger suppression of long-wavelength modes due to the dissipation. The onset of the κ^2 infrared scaling shifts to larger κ/κ_ζ as γ increases and α, κ_ζ decrease.

These properties on Ω_{gw} for monochromatic $\mathcal{P}_\zeta$ have the same physical origin as those for scale-invariant $\mathcal{P}_\zeta$, that is, the shorten of the lifetime of GW sources. Below, we analyze respectively how dissipative effects modifies the above three properties of Ω_{gw} for monochromatic $\mathcal{P}_\zeta$. Here, we still consider the approximation in Eq. (2.34), which enables us to make the most use of the analytical expression in Eq. (2.31) with $u = v = \kappa_\zeta/\kappa$. Thus, compared to Ref. [27], we provide a more intuitive analysis and do not require the power-law scaling of $\kappa_D(\hat{\tau})$.

(i) The sharp peak at $\kappa = (2/\sqrt{3})\,\kappa_\zeta$ arises from the resonant amplification of scalar perturbations, where $1/\sqrt{3}$ is the sound speed and the factor 2 comes from the second-order effect. To carefully discuss the divergence of this peak, we examine the behavior of Eq. (2.31) near the peak, i.e., $u = v \to \sqrt{3}/2$, and find it is dominated by the following terms

$$\mathcal{I}(u,v,\kappa,\hat{\tau}) \sim -\mathrm{Ci}\left(\left|1 - \frac{2u}{\sqrt{3}}\right|\kappa\hat{\tau}\right) + \ln\left(\left|1 - \frac{2u}{\sqrt{3}}\right|\right). \tag{3.11}$$

In the dissipation-free case, we usually consider the limit $\kappa\hat{\tau} \to \infty$ in Eq. (3.11), where the cosine-integral term vanishes while the leaving logarithmic singularity results in a divergent peak [3] [19]. However, the situation is differenet in the presence of dissipation. Considering the finite lifetimes of GW sources, the cosine-integral term cannot be neglected. Particularly, in the limits of $u = v \to \sqrt{3}/2$ and $\hat{\tau} \to \hat{\tau}_l(\kappa_\zeta, \alpha, \gamma)$, this cosine-integral term will tend to infinity and cancel out the logarithmic divergence term, ultimately giving a finite result

$$\mathcal{I}[u = v \to \sqrt{3}/2, \kappa, \hat{\tau} \to \hat{\tau}_l(\kappa_\zeta, \alpha, \gamma)] \sim -\gamma_E - \ln[\kappa\hat{\tau}_l(\kappa_\zeta, \alpha, \gamma)]. \tag{3.12}$$

---

[3]This divergence may be kind of subtle, because $\left|1 - \frac{2u}{\sqrt{3}}\right|\kappa\hat{\tau}$ here is actually a "$0 \cdot \infty$"-type indeterminate form. Anyway, this divergent peak usually does not cause serious disasters, since it is integrable and will disappears when replacing the unphysical Dirac-function $\mathcal{P}_\zeta$ by a realistic one with finite spectral width.

Here, we have used the relation

$$\lim_{x \to 0} [\, \mathrm{Ci}(x) - \ln x \,] = \gamma_E \; . \tag{3.13}$$

According to Eq. (3.12), the peak at $\kappa = (2/\sqrt{3})\,\kappa_\zeta$ is always finite even for a Dirac-function $\mathcal{P}_\zeta$. Moreover, the suppression of this peak is more significant for larger dissipation (with smaller $\kappa \hat{\tau}_l(\kappa_\zeta, \alpha, \gamma)$ in Eq. (3.12)).

(ii) Different from (i), the sharp valley at $\kappa = \sqrt{2/3}\,\kappa_\zeta$ is due to resonant cancellation of scalar perturbations. With dissipation, the reason of the disappearance of this valley is easy to point out: In Eq. (2.31), $u = v = \sqrt{3/2}$ is the solution of $\mathcal{I}(u, v, \kappa, \hat{\tau}) = 0$ only for $\kappa \hat{\tau} \to \infty$. If the lifetimes of GW sources are not sufficient large, the $\mathcal{O}(1/(\kappa \hat{\tau}))$ terms in Eq. (2.31) cannot be neglected, making $\kappa = \sqrt{2/3}\,\kappa_\zeta$ no longer a zero point of Ω_{gw}.

(iii) The infrared behavior of IGW spectrum is dependent on $\mathcal{I}(u, v, \kappa, \hat{\tau})$ in the limit $u = v = \kappa_\zeta/\kappa \gg 1$, whose leading terms are given by

$$\mathcal{I}(u, v, \kappa, \hat{\tau}) \sim \frac{1}{u^2} \left[\mathrm{Ci}\left(\kappa \hat{\tau} \right) + \ln\left(\frac{2u}{\sqrt{3}} \right) \right] \; , \tag{3.14}$$

Without dissipation, we can ignore the cosine-integral terms in the limit $\kappa \hat{\tau} \to \infty$, leading to $\mathcal{I} \sim u^{-2} \ln u$. Therefore, the IGW spectrum in the infrared region behaves as $\Omega_{\mathrm{gw}} \sim (u^{-2} \ln u)^2 |_{u=\kappa_\zeta/\kappa} \times (\kappa_\zeta/\kappa)^2 \sim \kappa^2 \ln^2 \kappa$. In the presence of dissipation, similar to (i), the modification of the infrared behavior also comes from the important contribution of cosine-integral terms in Eq. (3.14). Taking $\hat{\tau} \to \hat{\tau}_l(\kappa_\zeta, \alpha, \gamma)$, Eq. (3.14) is roughly given by

$$\mathcal{I}[u = v \gg 1, \kappa \gg \kappa_\zeta, \hat{\tau} \to \hat{\tau}_l(\kappa_\zeta, \alpha, \gamma)]$$
$$\sim \frac{1}{u^2} \left\{ \mathrm{Ci}\left[\frac{\kappa}{\kappa_\zeta} \kappa_\zeta \hat{\tau}_l(\kappa_\zeta, \alpha, \gamma) \right] - \ln\left(\frac{\sqrt{3}\,\kappa}{2\,\kappa_\zeta} \right) \right\} \sim \frac{1}{u^2} \left\{ \gamma_E + \ln\left[\frac{2\,\kappa_\zeta \hat{\tau}_l(\kappa_\zeta, \alpha, \gamma)}{\sqrt{3}} \right] \right\} \; , \tag{3.15}$$

where we have used Eq. (3.13) in the last step. Considering that $\kappa_\zeta \hat{\tau}_l(\kappa_\zeta, \alpha, \gamma)$ is not dependent on κ, Eq. (3.15) gives $\mathcal{I} \sim u^{-2}$ without the logarithmic running, and the IGW spectrum behaves as $\Omega_{\mathrm{gw}} \sim (u^{-2})^2 |_{u=\kappa_\zeta/\kappa} \times (\kappa_\zeta/\kappa)^2 \propto \kappa^2$ for $\kappa/\kappa_\zeta \to 0$. Furthermore, from Eq. (3.15), it is easy to find the transition point from $\sim \kappa^2 \ln^2 \kappa$ scaling to $\sim \kappa^2$ scaling is determined by the following parameter

$$\kappa_\zeta \hat{\tau}_l(\kappa_\zeta, \alpha, \gamma) = \gamma^{-2/\alpha} \kappa_\zeta^{1-2/\alpha}. \tag{3.16}$$

Given smaller $\kappa_\zeta \hat{\tau}_l(\kappa_\zeta, \alpha, \gamma)$, Eq. (3.15) could hold for larger κ/κ_ζ, so the onset of the κ^2 scaling shifts to larger κ/κ_ζ for increasing γ and decreasing α, κ_ζ. These properties are consistent with the numerical results in Fig. 6.

3.3 Log-normal curvature power spectrum

In this subsection, we consider that ζ has a log-normal primordial curvature power spectrum

$$\mathcal{P}_\zeta(\kappa) = \frac{\mathcal{A}_\zeta}{\sqrt{2\pi}\sigma} \, e^{-\frac{1}{2\sigma^2} \ln^2(\kappa/\kappa_\zeta)} \; , \tag{3.17}$$
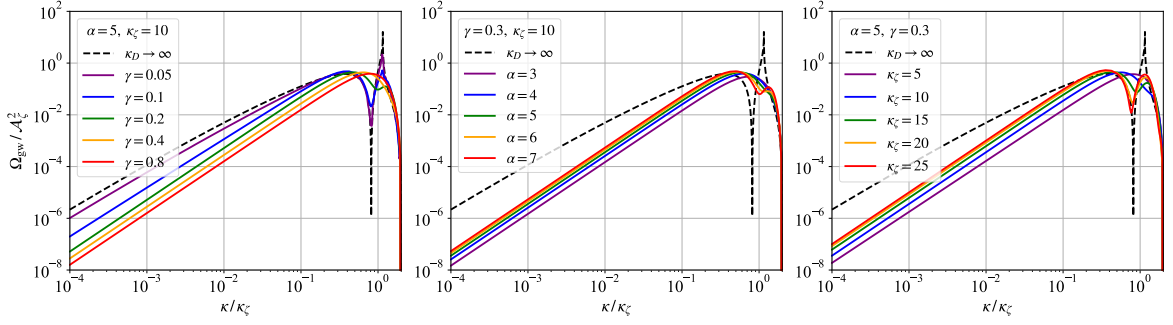
Figure 6. Energy-density spectrum Ω_{gw} normalized by $\mathcal{A}_\zeta^2$ versus the scale κ/κ_ζ for monochromatic primordial curvature power spectra. In the left panel, we fix $\alpha = 5$, $\kappa_\zeta = 10$ and take $\gamma = 0.05, 0.1, 0.2, 0.4, 0.8$. In the middle panel, we fix $\gamma = 0.3$, $\kappa_\zeta = 10$ and take $\alpha = 3, 4, 5, 6, 7$. In the right panel, we fix $\alpha = 5$, $\gamma = 0.3$ and take $\kappa_\zeta = 5, 10, 15, 20, 25$.

where κ_ζ gives the peak wavenumber, $\mathcal{A}_\zeta$ is the spectral amplitude at κ_ζ, and σ represents the spectral width. It could model a peaked spectrum with a finite width, and can be considered as a compromise between the previous two extreme cases. In the dissipation-free case, the IGW spectrum also presents as a wide peak with $\Omega_{\text{gw}}^{\kappa_D \to \infty} \sim \mathcal{A}_\zeta^2/(2\pi\sigma^2)$ at $\kappa \sim \kappa_\zeta$ and $\Omega_{\text{gw}}^{\kappa_D \to \infty} \sim \kappa^3 \ln^2 \kappa$ in the infrared region.

Fig. 7 and Fig. 8 show dissipative effects in IGWs for a log-normal $\mathcal{P}_\zeta$, focusing on the roles of the dissipation parameters γ and α, respectively. In each figure, the left and right columns respectively depict the IGW spectra normalized by $\mathcal{A}_\zeta^2$ and $\Omega_{\text{gw}}^{\kappa_D \to \infty}$, and the four rows from top to bottom depict the cases where the peaks of $\mathcal{P}_\zeta$ locate at $\kappa_\zeta = 1, 5, 10, 100$. We set $\sigma = 1$ for all above cases. As shown in Fig. 7 and Fig. 8, dissipative effects in this case exhibit combined properties of those in Section 3.1 and can also be modified by the shape of $\mathcal{P}_\zeta$ itself. We analysis them as follows.

(i) If dissipative effects happen in the "peak region" (i.e., $\kappa_\zeta \sim 1$), they are mainly manifested as amplitude suppression in $\kappa \gtrsim 1$, while the change in the infrared region is relatively small [4]. Particularly, they generally lead to a similar peak/valley structure with the case of scale-invariant $\mathcal{P}_\zeta$, that is, the dependence of these peaks/valleys's positions on α and γ are approximately the same, and we can also observe two notable valleys at $\kappa \sim \mathcal{O}(1)$ and $\kappa \gtrsim \mathcal{O}(10)$. Obviously, these peaks/valleys also arise from the oscillation of GW sources within their dissipation-induced lifetimes. Since Ω_{gw} in this "peak region" is mainly contributed by $u, v \sim 1$, we can conduct an analysis almost identical to that in Section 3.1 using $\omega_{\text{gw}}^{\kappa_D \to \infty}(1, 1, \kappa, \hat{\tau}_1, \hat{\tau}_2)$, except replacing the scale-invariant $\mathcal{P}_\zeta$ by the log-normal one. For a relatively wide $\mathcal{P}_\zeta$, this replacement does not significantly change of the peaks/valleys's positions, but only adjusts their shapes.

(ii) If dissipative effects happen at the "infrared region" (i.e., $\kappa_\zeta \gg 1$), the valley at

---

[4]The properties of dissipative effects for $\kappa_\zeta \ll 1$ are similar to those in the "peak region". We do not include $\kappa_\zeta \ll 1$ in our plots since $\Omega_{\text{gw}}(\kappa \gtrsim 1)$ is too small in this case.
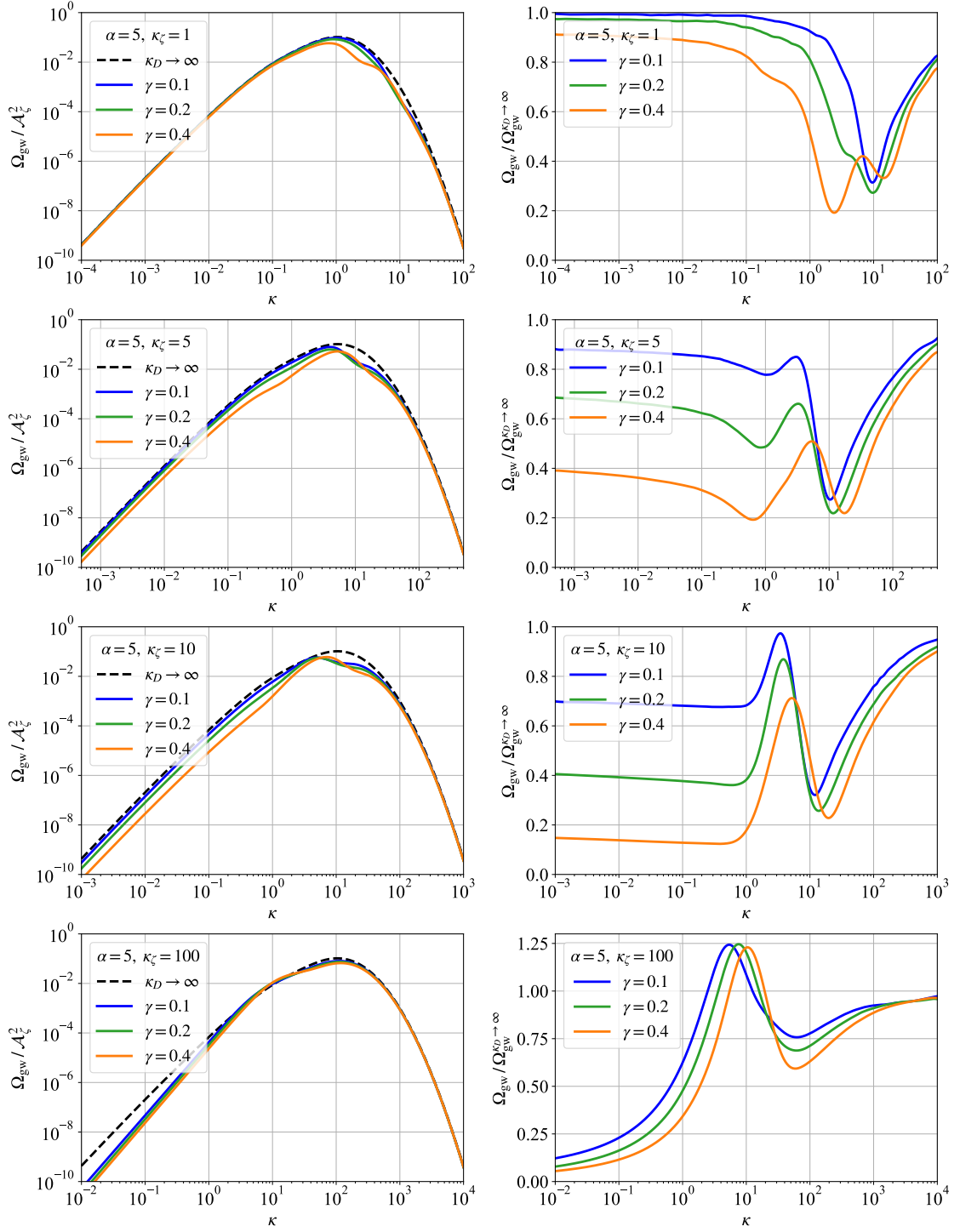
Figure 7. Energy-density spectrum Ω_{gw} normalized by $\mathcal{A}_\zeta^2$ (left column) and normalized by $\Omega_{\mathrm{gw}}^{\kappa_D \to \infty}$) (right column) versus the scale κ for log-normal primordial curvature power spectra. In both panels, we fix $\alpha = 5$ and take $\gamma = 0.1, 0.2, 0.4$. From the first to the fourth row, we respectively take $\kappa_\zeta = 1, 5, 10, 100$.
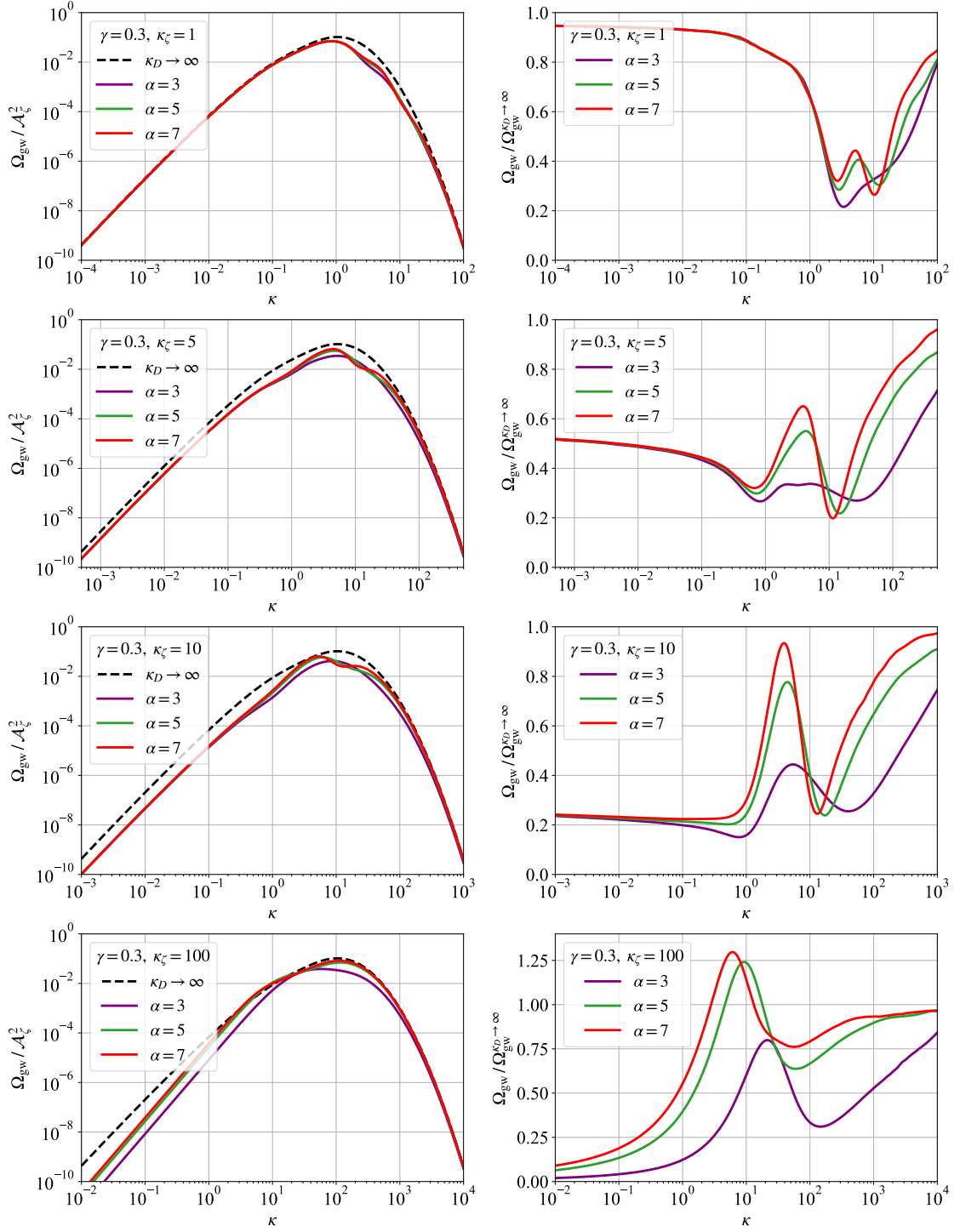
Figure 8. Energy-density spectrum Ω_{gw} normalized by $\mathcal{A}_\zeta^2$ (left column) and normalized by $\Omega_{\mathrm{gw}}^{\kappa_D \to \infty}$) (right column) versus the scale κ for log-normal primordial curvature power spectra. In both panels, we fix $\gamma = 0.3$ and take $\alpha = 3, 5, 7$. From the first to the fourth row, we respectively take $\kappa_\zeta = 1, 5, 10, 100$.
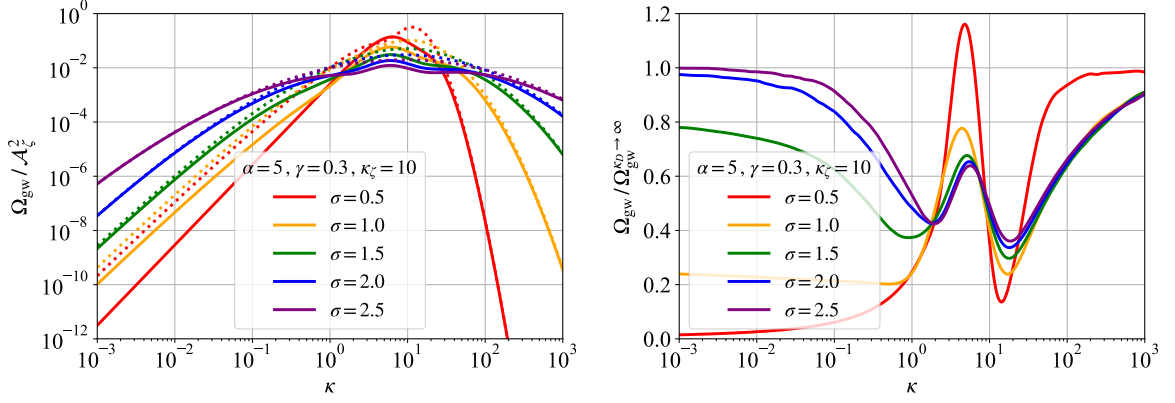
Figure 9. Energy-density spectrum Ω_{gw} normalized by $\mathcal{A}_\zeta^2$ (left panel) and normalized by $\Omega_{\mathrm{gw}}^{\kappa_D \to \infty}$) (right panel) versus the scale κ for log-normal primordial curvature power spectra. In both panels, we fix $\alpha = 5$, $\gamma = 0.3$, $\kappa_\zeta = 10$, and take $\sigma = 0.5, 1.0, 1.5, 2.0, 2.5$.

$\kappa \sim \mathcal{O}(1)$ may not appear (but the valley at $\kappa \sim \mathcal{O}(10)$ still exists). Instead, the infrared behavior $\Omega_{\mathrm{gw}}^{\kappa_D \to \infty} \sim \kappa^3 \ln \kappa^2$ is replaced by a steeper $\Omega_{\mathrm{gw}} \sim \kappa^3$ running at $\kappa \lesssim 1$. The origin of the disappearance of this logarithmic running is the same as discussed in Section 3.2, that is, considering the finite lifetimes of GW sources, the logarithmic term and the cosine-integral term in the $\mathcal{I}(u \gg 1, v \gg 1, \kappa < 1 \ll \kappa_\zeta, \hat{\tau} \to \hat{\tau}_l)$ would cancel each other out. It is noted that the infrared behavior of k^3 is usually regarded as a universal property of the SGWB, as required by causality [30]. After taking dissipative effects into account, our results, to a certain extent, restore this universal property.

(iii) If dissipative effects happen at the "intermediate region" between the above two, they only suppress the amplitude of Ω_{gw} at $\kappa \lesssim 1$, without altering its logarithmic running behavior. Different from (i) and (ii), in this region, the IGWs are not simply dominated by $u, v \sim 1$ or $u, v \gg 1$, but the contributions of both cannot be ignored. In Fig. 7 and Fig. 8, row 1 to 4 show the gradual transition process from the "peak region" to "infrared region", and the case $\kappa_\zeta \sim 10$ roughly corresponds to the "intermediate region". Besides, we should also note that the specific scope of the "intermediate region" should be determined by $\mathcal{P}_\zeta$. To demonstrate this, we plot in Fig. 9 the dissipation effects for different spectral widths σ, fixing $\kappa_\zeta = 10$, $\alpha = 5$, and $\gamma = 0.3$. For a wider $\mathcal{P}_\zeta$ (e.g., $\sigma = 2.5$), the case $\kappa_\zeta = 10$ corresponds to the typical "peak region", while for a narrower $\mathcal{P}_\zeta$ (e.g., $\sigma = 0.5$), it belongs to the "infrared region". These results reflect that dissipative effects in IGWs have a considerable dependence on the shape of $\mathcal{P}_\zeta$ itself.

At the end of this section, we summarize the basic properties of dissipation effects in IGWs as follows, based on the study of the above specific examples. Dissipative effects are most significant around $\kappa \sim 1$, corresponding to the horizon scale at the decoupling of weakly-interacting particles. Dissipative effects can leave characteristic imprints on the

IGW spectrum $\Omega_{\rm gw}$, including a notable suppression at $\kappa \sim 1$ and a modification of infrared behavior at $\kappa \lesssim 1$. The specific phenomenology largely depends on the shape of $\mathcal{P}_\zeta$ near $\kappa \sim 1$, and is also affected by the dissipation parameters α and γ. For a relatively flat $\mathcal{P}_\zeta$, the main effect of dissipation is to cause a suppression with a typical double-valley structure at $\kappa \sim 1$. This structure can be regarded as the characteristic that distinguishes dissipative effects from other physical mechanisms. Besides, the positions and amplitudes of the valleys are related to α and γ. For a narrow $\mathcal{P}_\zeta$, since $\Omega_{\rm gw}$ is greatly influenced by $\mathcal{P}_\zeta$ itself, dissipation effects at $\kappa \gtrsim 1$ are usually more complex and model-dependent (In an extreme of monochromatic $\mathcal{P}_\zeta$, dissipation effects smooth out the resonant peaks/valleys on $\Omega_{\rm gw}$). However, a relatively universal property of dissipation effects is that, they can remove the logarithmic running of the infrared behavior, replacing it by a pure power-law running. This infrared behavior is independent of the shape of $\mathcal{P}_\zeta$ and the dissipation parameters, but the onset scale at which the logarithmic running disappear is related to them. This property can also be regarded as a typical feature of the dissipative effect. From a physical perspective, the above results stem from the interaction between the dynamics of GW sources and dissipation effects, and can be intuitively explained by the "dissipation-induced lifetime" of GW sources.

4   Physical implications

Dissipation effects could introduce rich phenomenology on IGW spectrum, providing a new window into understanding the early universe. This section mainly discusses the implications of dissipative effects in the following two aspects. In Section 4.1, we will discuss the significant impacts of dissipation effects on GW observations. We emphasize that dissipation, as an intrinsic nature of cosmic fluid, is a basic factor to be considered in future GW analyses. In Section 4.2, we will focus on the connection between dissipative effects and particle interactions. We propose that dissipative effects in IGWs can provide a new framework for detecting fundamental physics at extremely high energy scales.

4.1   For gravitational-wave observations

To contact our theoretical results to GW observations, we need to know the present-day energy-density fraction spectrum $\Omega_{\rm gw,0}$. It can be obtained from $\Omega_{\rm gw}$ after considering the redshift of radiation components and the change of the relativistic degrees of freedoms in the early Universe, i.e.,

$$\Omega_{\rm gw,0}(f) = \Omega_{\rm rad,0} \left[\frac{g_{*,\rho}(T_{\rm e})}{g_{*,\rho}(T_{\rm eq})} \right] \left[\frac{g_{*,s}(T_{\rm eq})}{g_{*,s}(T_{\rm e})} \right]^{4/3} \Omega_{\rm gw}(k)|_{k\simeq 2\pi f} \,. \qquad (4.1)$$

Here, $f \simeq k/(2\pi)$ is the GW frequency, $\Omega_{\rm rad,0} = 4.2 \times 10^{-5}/h^2$ is the present-day energy-density fraction of radiations with $h = 0.674$ the dimensionless Hubble constant [22], $g_{*,\rho}$ (or $g_{*,\rho}$) is the effective relativistic degrees of freedom associated with the energy density (or
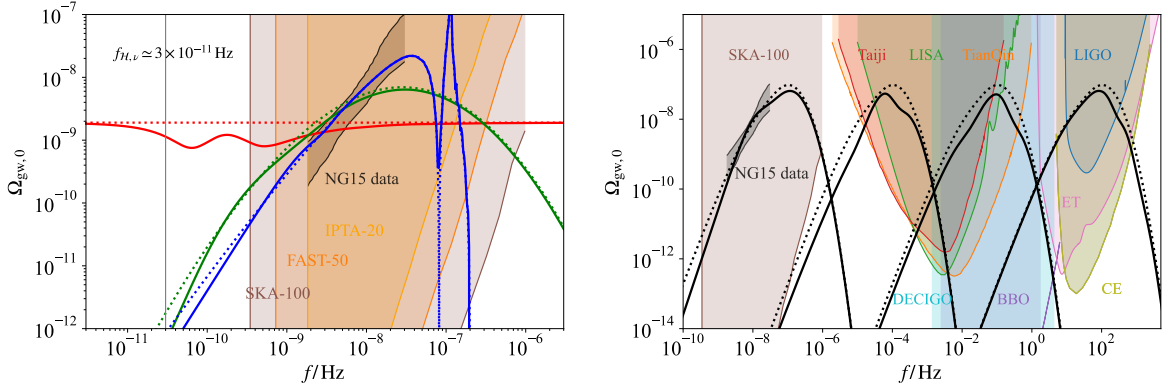
Figure 10. Present-day energy-density fraction spectrum $\Omega_{\text{gw},0}$ with (solid lines) and without (dotted lines) dissipation versus the GW frequency. Left panel: The red, blue, and green lines represent the results for scale-invariant $\mathcal{P}_\zeta$ (with $\mathcal{A}_\zeta = 0.005$), monochromatic $\mathcal{P}_\zeta$ (with $\mathcal{A}_\zeta = 0.025$ and $f_\zeta = 10^{-7}\,\text{Hz}$), and log-normal $\mathcal{P}_\zeta$ (with $\mathcal{A}_\zeta = 0.05$, $\sigma = 2$, and $f_\zeta = 3 \times 10^{-8}\,\text{Hz}$), respectively. Dissipation is caused by neutrinos, which is characterized by $\alpha \simeq 5$, $\gamma \simeq 0.3$, and $f_{\mathcal{H},\nu} \simeq 3 \times 10^{-11}\,\text{Hz}$. Right panel: The black lines represent the results for log-normal $\mathcal{P}_\zeta$ with $\mathcal{A}_\zeta = 0.1$, $\sigma = 1$, and $f_\zeta = 10^{-7}, 10^{-4}, 10^{-1}, 10^2\,\text{Hz}$ (from left to right). Dissipation is caused by possible new weakly-interacting particles X, where we set $\alpha \simeq 5$, $\gamma \simeq 0.3$, and $f_\zeta/f_{\mathcal{H},X} = 100, 10, 5, 1$ (from left to right).

entropy), and T_e (or T_{eq}) is the cosmic temperature at the GW emission (or matter-radiation equality) [31].

As the most basic observable for IGWs, $\Omega_{\text{gw},0}$ plays a central role in the analysis of observational data. Therefore, the precise theoretical calculation of $\Omega_{\text{gw},0}$ is of essential importance to connect GW observables with the early Universe. This calculation inevitably requires us to take dissipation effects into account in the study of IGWs. This is because that dissipative effects not only universally exist in cosmic fluid, but also become particularly significant near the decoupling of weakly-interacting particles, greatly affecting $\Omega_{\text{gw},0}$ in the relevant frequency bands. Our study of dissipative effects provide a more realistic template for $\Omega_{\text{gw},0}$, which has important implications for future GW observations, as discussed in the following.

Firstly, let us focus on the dissipative effects within the SM, which are dominated by weak-interaction of neutrinos, as formulated in Eq. (2.5). In this case, the dissipation parameters are given by $\alpha \simeq 5$ and $\gamma \simeq 0.3$, and the frequency corresponding to the horizon scale at neutrino decoupling is estimated as $f_{\mathcal{H},\nu} \simeq k_{\mathcal{H},\nu}/(2\pi) \simeq 3 \times 10^{-11}\,\text{Hz}$. In the left panel of Fig. 10, we plot the results of $\Omega_{\text{gw},0}$ with (solid lines) and without (dotted lines) dissipative effects, and compare them with the sensitivity curvies of IPTA (NANOGrav [6], European Pulsar Timing Array (EPTA) [7], and Parkes Pulsar Timing Array (PPTA) [8] combined), Five-Hundred-Meter Aperture Spherical Radio Telescope (FAST) [32], and Square Kilometre Array (SKA) [33]) for a 20-, 50-, and 100-year observation [34], respectively. As a result, dissipative effects would become significant around nano-hertz band, which will

be an important observational objective for PTA experiments. For example, for a scale-invariant $\mathcal{P}_\zeta = 0.005$ (red solid line), the corresponding $\Omega_{\mathrm{gw},0}$ will be suppressed dissipation effects by several tens of percent within the PTA frequency band (maximally by $\simeq 60\%$ at $f \simeq 0.5\,\mathrm{nHz}$). In particular, the characteristic valley structure at $f \simeq 0.5\,\mathrm{nHz}$ caused by neutrino decoupling can also be detected in future PTA experiments. Once detected, it will not only verify dissipative effects in IGWs, but also provide the unique feature for IGWs that distinguish them from other potential nanohertz GW sources (e.g., supermassive black hole binaries), helping us differentiate the components of SGWB. Our results indicate that, even within the SM, dissipative effects are of great significance to GW observations.

Since IGWs are the candidate for the GW signals reported by PTAs [21], it is essential to consider the impact of dissipation effects on PTA data analysis. As an illustration, in the left panel of Fig. 10, we plot the blue and green lines as possible interpretations of the NANOGrav 15-year (NG15) data [10] (gray region), where the blue (or green) lines correspond to the monochromatic (or log-normal) $\mathcal{P}_\zeta$ with $\mathcal{A}_\zeta = 0.025$ and $f_\zeta = 10^{-7}\,\mathrm{Hz}$ (or, $\mathcal{A}_\zeta = 0.05$, $\sigma = 2$, and $f_\zeta = 3 \times 10^{-8}\,\mathrm{Hz}$). For the narrow $\mathcal{P}_\zeta$, dissipation effects caused bu neutrino decoupling happen in the far-infrared region. The frequency band at which they significantly modify the infrared behavior of $\Omega_{\mathrm{gw},0}$ is slightly below the nanohertz band, making it difficult to be observed in current PTA experiments. However, for the wide $\mathcal{P}_\zeta$, we find that these dissipative effects could visibly change $\Omega_{\mathrm{gw},0}$ at $f \gtrsim \mathrm{nHz}$, thereby affecting the analysis of GW data. We leave the quantitative discussion to the future work. As the observation duration increases, it is expected that the PTAs experiment will detect GWs at lower frequencies, thus enabling a more comprehensive study of these dissipative effects caused by neutrinos.

Furthermore, we can consider the dissipative effects caused by underlying new physics. If there exist new paritcles X with weaker interaction than neutrinos, they would decouple earlier and the corresponding dissipative effects happen at higher frequencies. In the right panel of Fig. 10, we plot the results of $\Omega_{\mathrm{gw},0}$ for a log-normal $\mathcal{P}_\zeta$ with (solid lines) and without (dotted lines) dissipative effects, where we take $f_\zeta = 10^{-7}, 10^{-4}, 10^{-1}, 10^2\,\mathrm{Hz}$ and $f_\zeta / f_{\mathcal{H},X} = 100, 10, 5, 1$ from left to right, and fix $\mathcal{A}_\zeta = 0.1$, $\sigma = 1$, $\alpha = 5$, and $\gamma = 0.3$. In these case, dissipative effects in IGWs, including the characteristic suppression and the transition of infrared behavior, are expected to be detected by a wide range of GW experiments, such as PTA experiments (e.g., NANOGrav [6] and SKA [33]), space-based GW interferometers (e.g., LISA [35–37], Taiji [38], TianQin [39], Deci-hertz Interferometer Gravitational Wave Observatory (DECIGO) [40, 41], Big Bang Observer (BBO) [42, 43]), and ground-based GW interferometers (e.g., LIGO [1], Einstein Telescope (ET) [44], and Cosmic Explorer (CE) [45]). Their implications for new physics searches will be discussed in Section 4.2.

The infrared behavior of $\Omega_{\mathrm{gw},0}$ is the key information of SGWB. As for IGWs, their universal logarithmic infrared running is regarded as a unique feature to distinguish them from other sources [30, 46–51]. This property actually comes from the sufficiently long

lifetimes of the sources of IGWs. However, the situation becomes more complex in the presence of dissipation. Roughly speaking, this logarithmic running remains unchanged if dissipative effects happen in the "peak region", but disappers if they happen in the typical "infrared region", As stated in Section 3. Moreover, a complete analysis of the infrared behavior will be related to both the shape $\mathcal{P}_\zeta$ and the dissipation parameters. Our work emphasizes that, to describe the infrared behavior of IGWs more realistically, it is necessary to consider dissipative effects.

In addition to reshaping the profile of $\Omega_{\mathrm{gw},0}$, dissipative effects inherently lead to a reduction in the total energy density of IGWs, i.e., $\int \Omega_{\mathrm{gw},0}(f)\,\mathrm{d}\ln f$. For instance, in the case of a log-normal $\mathcal{P}_\zeta$ with $\sigma = 1$, the total GW energy fraction in the dissipation-free case is $\simeq 2.03 \times 10^{-5}\,\mathcal{A}_\zeta^2$. When dissipative effects are included (e.g., with $\alpha = 5$, $\gamma = 0.3$, and $f_\zeta/f_{\mathcal{H},j} = 1$), this value is reduced to $\simeq 1.31 \times 10^{-5}\,\mathcal{A}_\zeta^2$. Such reduction has noteworthy cosmological implications, as the big-bang nucleosynthesis and the CMB constrain the total energy density of extra relativistic species like GWs [52, 53] and therefore set bounds on $\mathcal{A}_\zeta$. As a result, dissipative effevts can release these bounds compared to the dissipation-free case.

4.2 For new physics searches

An important application of dissipative effects in IGWs is their use as a probe for new physics, owing to their close connection with particle interactions in the early Universe. Despite the SM's tremendous success in describing known particle interactions, unresolved issues such as neutrino masses and the matter-antimatter asymmetry strongly indicate the existence of the BSM physics. A common feature of many BSM scenarios is the introduction of extended gauge symmetries broken spontaneously at high energy scales, typically accompanied by additional heavy gauge bosons, whose masses may span many orders of magnitude. For instance, the grand unified theories (GUT) with gauge groups larger than $SU(5)$ generally predict additional gauge bosons, whose masses are allowed to range from the electroweak scale up to the GUT scale [54]. The detection of these heavy gauge bosons has essential implications for validating new physics scenarios. Yet, current and near-future collider experiments face significant challenges accessing energy scales well beyond the TeV range.

The early Universe, as a natural high-energy laboratory, offers a unique observational window to explore new physics. If new weakly-interacting particles X exist, their interactions with the cosmic plasma are expected to induce sizable dissipation upon decoupling in the early Universe. This dissipation is characterized by a damping scale $k_{D,X}$, which encodes key information about the underlying particle interactions. Correspondingly, these dissipative processes imprint distinctive signatures in the IGW spectrum at scales $k \sim k_{D,X}$, presenting detectable targets for future GW observations. Hence, dissipative effects in IGWs provide an indirect probe of new physics, especially at energy scales beyond the reach of traditional particle physics experiments. Building upon the initial proposal in Ref. [26], this work further develops this approach by enhancing the phenomenological understanding of dissipative

effects in IGWs. For a broad $\mathcal{P}_\zeta$, a characteristic suppression on $\Omega_{\rm gw}$, especially a multi-peak structure, if detected, serves as the fingerprint of the decoupling of some underlying weakly-interacting particles X, providing a smoking gun for new physics. The frequency location of this feature reveals the time of X-particle decoupling, which encodes the crucial information about their interactions. Moreover, the detailed shape of these spectral features enables us to extract the dissipation parameters α and γ, providing additional implications on the particle abundances and interactions. For a narrow $\mathcal{P}_\zeta$, identifying dissipative effects is usually more complex because $\Omega_{\rm gw}$ is largely shaped by $\mathcal{P}_\zeta$ itself. Nevertheless, the transition from $\sim k^n \ln k^2$ to $\sim k^n$ ($n = 2, 3$) in the infrared region could be a relatively general property in the presence of dissipation. Once detected, it also serves as typical signals of dissipative effects, suggesting the existence of new weakly-interacting particles. In the following, we mainly discuss on the former case.

To quantitatively present the detection potential to new physics at extremely high energy scales, we consider the interaction of weakly-interacting particles X parameterized by Eq. (2.5). In this example, the mass of the mediated gauge bosons, $M_{W'}$, corresponds to the energy scale of the related new physics. When these X-particles decouple in the early Universe, the damping scale is roughly estimated as $k_{D,X}/{\rm Mpc}^{-1} \sim 10^2 \ (M_{W'}/{\rm GeV})^{4/3}$, and the associated dissipative effects on $\Omega_{\rm gw,0}(f)$ occurs at frequencies approximately

$$f/{\rm Hz} \sim \mathcal{O}(1 - 10) \times 10^{-13} \ (M_{W'}/{\rm GeV})^{4/3} \ . \tag{4.2}$$

Based on Eq. (4.2), PTA experiments are projected to detect dissipative effects corresponding to the parameter space $M_{W'} \sim \mathcal{O}(10^3 - 10^4)\,{\rm GeV}$. This energy scale range is particularly noteworthy as it overlaps with the anticipated sensitivity of next-generation colliders, offering valuable cross-check with experiments such as Large Hadron Collider (LHC), Future Circular Collider (FCC) [55], International Linear Collider (ILC) [56], and Circular Electron Positron Collider (CEPC) [57–59]. Space-based gravitational wave interferometers probe higher energy scales, corresponding to $M_{W'} \sim \mathcal{O}(10^7 - 10^9)\,{\rm GeV}$, while ground-based GW interferometers extend the sensitivity up to $M_{W'} \sim \mathcal{O}(10^{10} - 10^{12})\,{\rm GeV}$. These scales far exceed the reach of terrestrial collider experiments, yet offer valuable opportunities to explore new physics through cosmic observations. Complementary observations come from high-energy cosmic ray experiments, such as Pierre Auger Observatory (PAO) [60], Telescope Array (TA) [61], and Large High Altitude Air Shower Observatory (LHAASO) [62]. We expect that such multi-messenger search could scan a wide range of energy scales, enriching our capability to explore new physics.

We note that since $\mathcal{P}_\zeta$ is unknown a priori, there may be some uncertainties in the realistic analysis of dissipative effects in IGWs. However, we would like to emphasize the robustness of this approach by discussing the following aspects about $\mathcal{P}_\zeta$.

- Position of k_ζ: To detect dissipative effects, we at least require large enough $\mathcal{P}_\zeta$ at relevant scales to generate observable IGWs. For such $\mathcal{P}_\zeta$, the relative position between

its typical scale k_ζ and damping scale $k_{D,X}$ significantly influences the manifestation of dissipative effects in IGWs. Obviously, the suppression in $\Omega_{\rm gw}$ is more pronounced when k_ζ is closer to $k_{D,X}$. However, we observe that even if k_ζ and $k_{D,X}$ differ significantly (e.g., $k_\zeta/k_{D,X} \sim 10^2$), dissipative effects in IGWs remain notable enough, reducing $\Omega_{\rm gw}$ by several tens of percent, as shown in Section 3.3. This indicates that the detection of dissipative effects is feasible across a wide parameter space, without requiring exact scale matching.

- Shape of $\mathcal{P}_\zeta$: Though lacking the specific shape of $\mathcal{P}_\zeta$ makes it difficult to precisely measure dissipative effects, we emphasize that for our purpose of probing new physics, it is usually not a serious problem. This is because in our approach, the most robust and accessible observable is the feature's frequency, instead of its exact shape. As long as the dissipation-induced feature is identifiable, its frequency can be well measured, from which we can extract the particle interaction information even without the knowledge about $\mathcal{P}_\zeta$ (as shown in Eq. (4.2)). Moreover, the shape of dissipation-induced feature is more likely to be well measured for a relatively broad $\mathcal{P}_\zeta$, since it is less affected by $\mathcal{P}_\zeta$ itself. In this case, we can extract dissipation parameters α and γ and get further implications for the related new physics, e.g., the abundance of X-particles.

- Possible degeneracy: Features in $\Omega_{\rm gw}$ consistently attract significant attention as they strongly indicate the presence of nontrivial physical processes. As for IGWs, both dissipative effects and $\mathcal{P}_\zeta$ itself can generate features in $\Omega_{\rm gw}$ (for the latter, see Ref. [63] for a review). A natural question arises whether features from these two origins can be degenerate. Though the degeneracy cannot be theoretically ruled out, we emphasize that the unique characteristics of dissipation-induced features, most notably their multi-peak structure, distinguish them from features caused by other known physical scenarios, offering a promising means to identify particle decoupling in the early Universe. Furthermore, given that degeneracies often appear in GW cosmology, this motivates future research to incorporate complementary observables, such as GW anisotropies, which may help break potential degeneracies.

Although the generation of $\mathcal{P}_\zeta$ and the presence of new particles are usually independent, it is interesting that some cosmological models predict both simultaneously. For example, Ref. [64] considers a $U(1)$ gauge field kinetically coupled to an inflaton, which could copiously produce new heavy gauge bosons, and also enhance $\mathcal{P}_\zeta$ to $\sim 10^{-3}$. If the damping scale is determined by the gauge boson's mass through Eq. (4.2) and has overlap with the enhanced scales of $\mathcal{P}_\zeta$, the corresponding dissipative effects in IGWs are potentially detected by GW experiments. A detection of such effects could probe these new particles, while the non-detection can restrict the parameter space, providing an important test of this model. In principle, given such a new physics model, we can calculate the corresponding dissipative effects in IGWs following our flamework, and compare this template to the GW observations.

Our work may lay the foundation for future model-building efforts combining enhanced primordial perturbations and new particle content, an endeavor valuable both theoretically and observationally, which strengthens the interface between particle physics and cosmology.

In summary, dissipative effects in IGWs serve as characteristic features of the decoupling of weakly-interacting particles and encode rich information on their interactions. These effects provide a new framework to probe new physics at extremely high energy scales, advancing our understanding of the early Universe and fundamental physics.

5 Extended study

We have investigated dissipative effects in IGWs in the most standard case, that is, we assume primordial curvature perturbations ζ to be Gaussian, and only consider the energy-density spectrum of IGWs produced in the RD era. As an extended study, we here discuss some basic contents about the following three topics, while leave their detailed researches to future work. In Section 5.1, we study the dissipative effects in IGWs in the case that ζ deviate from Gaussian statistics, which is known as primordial non-Gaussianity. In Section 5.2, we consider the anisotropies in the IGW background caused by primordial non-Gaussianity, and study the role of dissipation here. In Section 5.3, we turn to IGWs related to the early matter-dominated (eMD) era, and focus how dissipation affects the so-called "poltergeist mechanism".

5.1 Dissipative effects in the presence of primordial non-Gaussianity

While the standard single-field slow-roll inflation predicts nearly Gaussian ζ, a broad range of inflation models (e.g., non-standard single-field inflation [65–73] or multi-field inflation [74–82]) can generate sizable primordial non-Gaussianity, which reflects the interactions of quantum fields during inflation. In this work, we consider the local-type non-Gaussianity, and expand ζ up to the F_{NL}-order as follows

$$\zeta_{\mathbf{k}} = \zeta_{g,\mathbf{k}} + F_{\mathrm{NL}} \int \frac{\mathrm{d}^3\mathbf{q}}{(2\pi)^{3/2}} \, \zeta_{g,\mathbf{k}-\mathbf{q}} \, \zeta_{g,\mathbf{q}} \,, \tag{5.1}$$

where ζ_g is the Gaussian component of ζ. Given the non-Gaussian ζ in Eq. (5.1), the IGW spectrum $\Omega_{\mathrm{gw}} \sim \langle\zeta^4\rangle$ can be expanded in terms of $\langle\zeta_g^2\rangle$ and finally recast as $\Omega_{\mathrm{gw}} = \Omega_{\mathrm{gw}}^{(0)} + \Omega_{\mathrm{gw}}^{(1)} + \Omega_{\mathrm{gw}}^{(2)}$, where $\Omega_{\mathrm{gw}}^{(m)}$ $(m = 0, 1, 2)$ stand for the $\mathcal{O}(\mathcal{A}_\zeta^{m+2} F_{\mathrm{NL}}^{2m})$ components of Ω_{gw}. The explicit expressions of $\Omega_{\mathrm{gw}}^{(m)}$ are given by [48, 83, 84]

$$\Omega_{\mathrm{gw}}^{(0)}(\kappa, \hat{\tau}) = \frac{1}{12} \int_{-1}^{1} \mathrm{d}s \int_{0}^{\infty} \mathrm{d}t \, uv \, \overline{J^2(u, v, \kappa, \hat{\tau})} \, \frac{\mathcal{P}_{\zeta_g}(v\kappa)}{v^3} \frac{\mathcal{P}_{\zeta_g}(u\kappa)}{u^3} \,, \tag{5.2}$$

$$\Omega_{\mathrm{gw}}^{(1)}(\kappa, \hat{\tau}) = \frac{1}{12} F_{\mathrm{NL}}^2 \int_{-1}^{1} \mathrm{d}s_1 \int_{0}^{\infty} \mathrm{d}t_1 \int_{-1}^{1} \mathrm{d}s_2 \int_{0}^{\infty} \mathrm{d}t_2$$

$$\times \left\{ u_1 v_1^4 u_2 v_2 \, \overline{J^2(u_1, v_1, \kappa, \hat{\tau})} \, \frac{\mathcal{P}_{\zeta_g}(u_1\kappa)}{u_1^3} \frac{\mathcal{P}_{\zeta_g}(v_2 v_1 \kappa)}{(v_2 v_1)^3} \frac{\mathcal{P}_{\zeta_g}(u_2 v_1 \kappa)}{(u_2 v_1)^3} \right.$$

$$+u_1 v_1 u_2 v_2 \, \overline{J(u_1, v_1, \kappa, \hat{\tau}) \, J(u_2, v_2, \kappa, \hat{\tau})} \times \int_0^{2\pi} \frac{\mathrm{d}\varphi_{12}}{\pi} \cos 2\varphi_{12}$$

$$\times \left[\frac{\mathcal{P}_{\zeta_g}(v_2\kappa)}{v_2^3} \frac{\mathcal{P}_{\zeta_g}(u_2\kappa)}{u_2^3} \frac{\mathcal{P}_{\zeta_g}(w_{12}\kappa)}{w_{12}^3} + \frac{\mathcal{P}_{\zeta_g}(v_1\kappa)}{v_1^3} \frac{\mathcal{P}_{\zeta_g}(v_2\kappa)}{v_2^3} \frac{\mathcal{P}_{\zeta_g}(w_{012}\kappa)}{w_{012}^3} \right] \right\} , \quad (5.3)$$

$$\Omega_{\mathrm{gw}}^{(2)}(\kappa, \hat{\tau}) = \frac{1}{48} F_{\mathrm{NL}}^4 \int_{-1}^1 \mathrm{d}s_1 \int_0^\infty \mathrm{d}t_1 \int_{-1}^1 \mathrm{d}s_2 \int_0^\infty \mathrm{d}t_2 \int_{-1}^1 \mathrm{d}s_3 \int_0^\infty \mathrm{d}t_3$$

$$\times \left\{ u_1^4 v_1^4 u_2 v_2 u_3 v_3 \, \overline{J^2(u_1, v_1, \kappa, \hat{\tau})} \, \frac{\mathcal{P}_{\zeta_g}(v_2 v_1 \kappa)}{(v_2 v_1)^3} \frac{\mathcal{P}_{\zeta_g}(u_2 v_1 \kappa)}{(u_2 v_1)^3} \frac{\mathcal{P}_{\zeta_g}(v_3 u_1 \kappa)}{(v_3 u_1)^3} \frac{\mathcal{P}_{\zeta_g}(u_3 u_1 \kappa)}{(u_3 u_1)^3} \right.$$

$$+ u_1 v_1 u_2 v_2 u_3 v_3 \, \overline{J(u_1, v_1, \kappa, \hat{\tau}) \, J(u_2, v_2, \kappa, \hat{\tau})} \times \frac{1}{2} \int_0^{2\pi} \frac{\mathrm{d}\varphi_{12}}{\pi} \int_0^{2\pi} \frac{\mathrm{d}\varphi_{23}}{\pi} \cos 2\varphi_{12}$$

$$\left. \times \frac{\mathcal{P}_{\zeta_g}(v_3\kappa)}{v_3^3} \frac{\mathcal{P}_{\zeta_g}(w_{13}\kappa)}{w_{13}^3} \frac{\mathcal{P}_{\zeta_g}(w_{23}\kappa)}{w_{23}^3} \left[2 \frac{\mathcal{P}_{\zeta_g}(u_3\kappa)}{u_3^3} + \frac{\mathcal{P}_{\zeta_g}(w_{0123}\kappa)}{w_{0123}^3} \right] \right\} , \quad (5.4)$$

with $J(u, v, \kappa, \hat{\tau}) = \left[v^2 - (1 + v^2 - u^2)^2/4 \right] \times \mathcal{I}(u, v, \kappa, \hat{\tau})$ [5]. Note that Eq. (5.2) just has the same form as the results in existing literature except that the $\mathcal{I}(u, v, \kappa, \hat{\tau})$ here includes dissipative effects.

In Fig. 11, the left panel plots the numerical results of $\Omega_{\mathrm{gw}}^{(m)}$ (nomarlized by $\mathcal{A}_\zeta^{m+2} F_{\mathrm{NL}}^{2m}$) with or without dissipative effects, and the right panel plots the ratio $\Omega_{\mathrm{gw}} / \Omega_{\mathrm{gw}}^{\kappa_D \to \infty}$ for different non-Gaussianity parameters $\mathcal{A}_\zeta F_{\mathrm{NL}}^2$. Here, we take the dissipation parameters as $\alpha = 5$ and $\gamma = 0.3$, and assume $\mathcal{P}_{\zeta_g}(\kappa)$ a log-normal spectrum with $\kappa_\zeta = 1$ and $\sigma = 1$. In the presence of primordial non-Gaussianity, we find that dissipative effects still result in a peak/valley structure on Ω_{gw}, whose location remains nearly unchanged comparing to the Gaussian case. The effect of non-Gaussianity is to change the contrast ratio of the dissipation-induced peak/valley structure, making it less obvious as the parameter $\mathcal{A}_\zeta F_{\mathrm{NL}}^2$ increases. It can be intuitively understood as follows: Since the non-Gaussianity introduces non-linear couplings between different scales, the damping of the mode $k \sim k_{D,j}$ also affect other modes. As a result, dissipative effects on Ω_{gw} located at $\kappa \sim \mathcal{O}(1-10)$ would "spread out" to other scales, thus reducing the contrast ratio of the features. This effect is quite different with those of dissipation parameters themselves, serving as distinctive signals of

---

[5]The notations in Eq. (5.2) are defined as follows

$$s_i = u_i - v_i \ ,$$

$$t_i = u_i + v_i - 1 \ ,$$

$$y_i = \frac{1}{2}[1 - s_i(t_i + 1)] \ ,$$

$$y_{ij} = \frac{\cos \varphi_{ij}}{4} \sqrt{t_i(t_i + 2)(1 - s_i^2)t_j(t_j + 2)(1 - s_j^2)} + \frac{1}{4}[1 - s_i(t_i + 1)][1 - s_j(t_j + 1)] \ , \quad (5.5)$$

$$w_{ij} = \sqrt{v_i^2 + v_j^2 - 2y_{ij}} \ ,$$

$$w_{012} = \sqrt{1 + v_1^2 + v_2^2 - 2y_1 - 2y_2 + 2y_{12}} \ ,$$

$$w_{0123} = \sqrt{1 + v_1^2 + v_2^2 + v_3^2 - 2y_1 - 2y_2 + 2y_3 + 2y_{12} - 2y_{23} - 2y_{31}} \ .$$
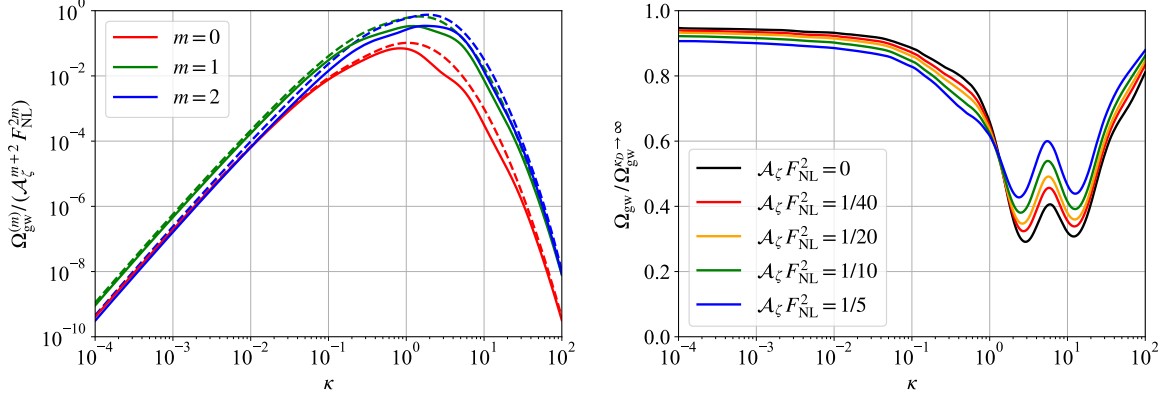
primordial non-Gaussianity.

Figure 11. Left panel: Non-Gaussian components of energy-density fraction spectrum, $\Omega_{\rm gw}^{(m)}$ (normalized by $\mathcal{A}_\zeta^{m+2} F_{\rm NL}^{2m}$, $m = 0, 1, 2$), versus the scale κ with (solid lines) and without (dashed lines) dissipation. Right panel: Total energy-density fraction spectrum $\Omega_{\rm gw}$ (normalized by the dissipation-free result $\Omega_{\rm gw}^{\kappa_D \to \infty}$) versus the scale κ for various values of $\mathcal{A}_\zeta F_{\rm NL}^2$. In both panels, we fix the dissipation parameters to $\alpha = 5$, $\gamma = 0.3$, and assume a log-normal primordial power spectrum with $\sigma = 1$ and $\kappa_\zeta = 1$ for ζ_g.

5.2 Anisotropies in the induced gravitational-wave background

Besides the isotropic component of SGWB described by $\Omega_{\rm gw}$, the anisotropies of SGWB are another important GW observable and could further bring us crucial information about the early Universe. The anisotropies are characterized by the reduced angular power spectrum $\widetilde{C}_\ell$, defined as the correlation of large-scale GW density contrasts $\delta_{{\rm gw},0,\mathbf{k}}$ along two lines-of-sight, i.e.,

$$\delta_{\ell_1 \ell_2} \delta_{m_1 m_2} \widetilde{C}_\ell(k) = \langle \delta_{{\rm gw},0,\ell_1 m_1}(k)\, \delta_{{\rm gw},0,\ell_2 m_2}^*(k) \rangle \ . \tag{5.6}$$

Here, $\mathbf{k}$ is the Fourier mode of GWs, $\delta_{{\rm gw},0,\ell m}$ is the spherical harmonic coefficient of $\delta_{{\rm gw},0,\mathbf{k}}$, namely, $\delta_{{\rm gw},0,\mathbf{k}} = \Sigma_{\ell m}\, \delta_{{\rm gw},0,\ell m}(k)\, Y_{\ell m}(\mathbf{k}/k)$. As for IGWs, the large-scale $\delta_{{\rm gw},0,\mathbf{k}}$ can be naturally generated by primordial non-Gaussianity [37, 50, 51, 84–93], since it can redistribute the IGW density through the coupling between large- and small-scale curvature perturbations. At a coarse-grained location $\mathbf{x}$, the large-scale $\delta_{{\rm gw},0,\mathbf{k}}$ of IGWs is given by [84]

$$\delta_{{\rm gw},0,\mathbf{k}}(\mathbf{x}) \simeq \left\{ F_{\rm NL}\, \frac{8\, \Omega_{\rm gw}^{(0)}(k) + 4\, \Omega_{\rm gw}^{(1)}(k)}{\Omega_{\rm gw}^{(0)}(k) + \Omega_{\rm gw}^{(1)}(k) + \Omega_{\rm gw}^{(2)}(k)} + \frac{3}{5}\left[4 - n_{\rm gw}(k)\right] \right\} \times \int \frac{{\rm d}^3 \mathbf{q}}{(2\pi)^{3/2}}\, e^{i\mathbf{q}\cdot\mathbf{x}}\, \zeta_{gL,\mathbf{q}} \ , \tag{5.7}$$

where $n_{\rm gw}(k) = \partial \ln \Omega_{\rm gw}(k)\, /\, \partial \ln k$ is the spectral index of $\Omega_{\rm gw}$, and ζ_{gL} is the large-scale curvature perturbations. In the right-hand side of Eq. (5.7), the first term is the density contrast of GWs at their emission arising from primordial non-Gaussianity, while the second term is known as the Sachs-Wolfe effect, corresponding to the redshift/blueshift of GWs during their propagation due to the existence of large-scale gravitational potential [94]. We here

do not include other propagation effects, which are expected to be negligible [85]. Combining Eq. (5.6) and Eq. (5.7), the $\widetilde{C}_\ell$ of the IGW background can be obtained as [84]

$$\ell(\ell + 1)\,\widetilde{C}_\ell(\kappa) = 2\pi\mathcal{A}_{\mathrm{L}}\left\{ F_{\mathrm{NL}}\,\frac{8\,\Omega_{\mathrm{gw}}^{(0)}(\kappa) + 4\,\Omega_{\mathrm{gw}}^{(1)}(\kappa)}{\Omega_{\mathrm{gw}}^{(0)}(\kappa) + \Omega_{\mathrm{gw}}^{(1)}(\kappa) + \Omega_{\mathrm{gw}}^{(2)}(\kappa)} + \frac{3}{5}\left[4 - n_{\mathrm{gw}}(\kappa)\right]\right\}^2, \qquad (5.8)$$

where $\mathcal{A}_{\mathrm{L}} \simeq 2.1 \times 10^{-9}$ is the spectral amplitude of ζ_{gL} given by CMB observations [22]. In Eq. (5.8), dissipative effects could affect the anisotropies of IGWs by modifying $\Omega_{\mathrm{gw}}^{(m)}(\kappa)$ ($m = 0, 1, 2$) as well as $n_{\mathrm{gw}}(\kappa)$.

We plot the $\ell(\ell + 1)\,\widetilde{C}_\ell(\kappa)$ in the left panel of Fig. 12, where the solid (or dashed) lines stand for the results with (or without) dissipation. Here, we adopt the same dissipation parameters and $\mathcal{P}_{\zeta_g}$ as those in Section 5.1. Dissipation only introduces some small fluctuations as n_{gw} in Eq. (5.8) is only slightly modified. As an important result, we note that the value of $\widetilde{C}_\ell$ is hardly affected by dissipative effects. This is because the first term on the right-hand side of Eq. (5.8) is largely insensitive to dissipation since dissipation alters the numerator and denominator in a compensating way. More physically, this result can be understood by the following fact: dissipative effects only happen inside the horizon, whereas the $\widetilde{C}_\ell$ cares about the physics on large scales. As an enlightening perspective, this result suggests that GW anisotropies could serve as a robust probe of the primordial Universe (e.g., primordial non-Gaussianity) that is largely immune to subhorizon physics such as dissipation. Regarding observations, we further define the angular power spectrum $C_\ell = [\Omega_{\mathrm{gw},0}/(4\pi)]^2\,\widetilde{C}_\ell$. Form the right panel of Fig. 12, we see that dissipative effects can suppress C_ℓ by roughly an order of magnitude around $\kappa \sim \mathcal{O}(1 - 10)$. This suppression is almost entirely due to the reduction of $\Omega_{\mathrm{gw},0}$, making the detection of GW anisotropies more challenging at those scales.
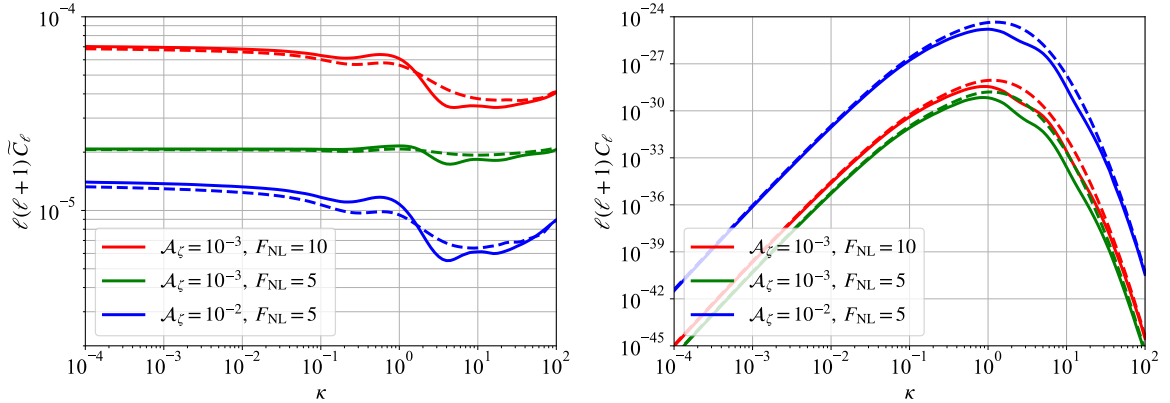

Figure 12. Left panel: Reduced angular power spectra $\ell(\ell + 1)\,\widetilde{C}_\ell$ versus the scale κ with (solid lines) or without (dashed lines) dissipation. Right panel: Angular power spectra $\ell(\ell+1)\,C_\ell$ versus the scale κ with (solid lines) or without (dashed lines) dissipation. In both panels, we fix the dissipation parameters to $\alpha = 5$, $\gamma = 0.3$, and assume a log-normal primordial power spectrum with $\sigma = 1$ and $\kappa_\zeta = 1$ for ζ_g.

5.3 Poltergeist mechanism

So far, all we consider is the IGWs in the standard RD Universe. However, the thermal history of Universe before big bang nucleosynthesis is lack of observational constraints, and many natural cosmological models predict the existence of an eMD era (e.g., see Ref. [95] for a review). If the transition from the eMD era to the RD era is rapid, IGWs can be dramatically produced through the "poltergeist mechanism" [96–98]. predict an eMD era, which with a rapid transition to the standard RD era. In this case, IGWs can be dramatically produced through the "poltergeist mechanism". For simplicity, we assume an instantaneous eMD-to-RD transition at τ_R. In this case, the scale factor and conformal Hubble parameter of the Universe are respectively given by

$$\frac{a(\tau)}{a(\tau_R)} = \begin{cases} (\tau/\tau_R)^2 \ , \ \tau \leq \tau_R \ , \\ 2(\tau - \tau_R/2)/\tau_R \ , \ \tau \geq \tau_R \ , \end{cases} \quad \text{and} \ \mathcal{H}(\tau) = \begin{cases} 2/\tau \ , \ \tau \leq \tau_R \ , \\ 1/(\tau - \tau_R/2) \ , \ \tau \geq \tau_R \ . \end{cases} \quad (5.9)$$

and, the evolution of $\phi_{\mathbf{k}}(\tau)$ can be described as

$$\phi_{\mathbf{k}}(\tau) = \begin{cases} \zeta_{\mathbf{k}} \times (3/5) \ , \ \tau \leq \tau_R \ , \\ \zeta_{\mathbf{k}} \times (2/3) \, \Phi_{\mathrm{RD}}(k,\tau) \simeq \zeta_{\mathbf{k}} \times (2/3) \, \Phi_{\mathrm{RD}}^{k_D \to \infty}(k,\tau) \, e^{-k^2/k_D^2(\tau)} \ , \ \tau \geq \tau_R \ , \end{cases} \quad (5.10)$$

where $\Phi_{\mathrm{RD}}^{k_D \to \infty}(k,\tau)$ is determined by the continuity of ϕ and ϕ' [6], and we take into account of the dissipative effects in the RD era while neglect those in the eMD era. Here, we assume that the damping scale $k_D(\tau)$ follows a power-law scaling for a period of time right after the eMD era, parameterized by α_R and γ_R, i.e.,

$$k_D(\tau) \, \tau_R = \gamma_R^{-1} \, (\tau/\tau_R)^{-\alpha_R/2} \ , \quad \tau > \tau_R \ . \quad (5.13)$$

We will focus on the IGW production during the RD era, which makes a leading contribution. Similar to Eq. (2.28), the GW spectrum $\Omega_{\mathrm{gw}} \simeq \Omega_{\mathrm{gw,RD}}$ can be calculated through the kernel

---

[6]The explicit expression of $\Phi_{\mathrm{RD}}^{k_D \to \infty}(k,\tau)$ is given by

$$\Phi_{\mathrm{RD}}^{k_D \to \infty}(k,\tau) = \frac{9}{10} \left\{ A \, \frac{3 \, j_1 \left[k(\tau - \tau_R/2)/\sqrt{3} \right]}{k(\tau - \tau_R/2)/\sqrt{3}} + B \, \frac{3 \, y_1 \left[k(\tau - \tau_R/2)/\sqrt{3} \right]}{k(\tau - \tau_R/2)/\sqrt{3}} \right\} \ , \quad (5.11)$$

where $j_1(x)$ (or $y_1(x)$) is the first (or second) kind of spherical Bessel function of order 1, and the coefficients A and B are respectively given by [96]

$$A = \frac{1}{36} \left\{ 6\sqrt{3} \, (k\tau_R) \sin\left(\frac{k\tau_R}{2\sqrt{3}} \right) - \left[(k\tau_R)^2 - 36 \right] \cos\left(\frac{k\tau_R}{2\sqrt{3}} \right) \right\} \ , \quad (5.12a)$$

$$B = -\frac{1}{36} \left\{ \left[(k\tau_R)^2 - 36 \right] \sin\left(\frac{k\tau_R}{2\sqrt{3}} \right) + 6\sqrt{3} \, (k\tau_R) \cos\left(\frac{k\tau_R}{2\sqrt{3}} \right) \right\} \ . \quad (5.12b)$$

function in the RD era, i.e.,

$$
\overline{\mathcal{I}_{\mathrm{RD}}^2}(u,v,k,\tau) = \int_{k\tau_R}^{k\tau} \mathrm{d}(k\tau_1) \int_{k\tau_R}^{k\tau} \mathrm{d}(k\tau_2) \times \frac{1}{2} \Bigg\{ \prod_{i=1,2} \left[(k\tau_i - k\tau_R/2) \cos(k\tau_i) f_{\mathrm{RD}}(uk,vk,\tau_i) \right]
$$
$$
+ \prod_{i=1,2} \left[(k\tau_i - k\tau_R/2) \sin(k\tau_i) f_{\mathrm{RD}}(uk,vk,\tau_i) \right] \Bigg\},
$$
(5.14)

where the source function f_{RD} is given by

$$
f_{\mathrm{RD}}(uk,vk,\tau_i) = \frac{4}{3} \Phi_{\mathrm{RD}}(uk,\tau_i) \Phi_{\mathrm{RD}}(vk,\tau_i) + \frac{4}{9} (\tau_i - \tau_R/2)^2 \Phi'_{\mathrm{RD}}(uk,\tau_i) \Phi'_{\mathrm{RD}}(vk,\tau_i)
$$
$$
+ \frac{4}{9} (\tau_i - \tau_R/2) \left[\Phi_{\mathrm{RD}}(uk,\tau_i) \Phi'_{\mathrm{RD}}(vk,\tau_i) + \Phi'_{\mathrm{RD}}(uk,\tau_i) \Phi_{\mathrm{RD}}(vk,\tau_i) \right].
$$
(5.15)

The "poltergeist mechanism" is physically explained as follows: For $\phi_{\mathbf{k}}$ with $k\tau_R \gg 1$, they keep as constant during the eMD era and turn to oscillate very fast (comparing to the cosmic expansion) once the RD era begins. If the eMD-to-RD transition is sufficiently rapid, the amplitudes of $\phi_{\mathbf{k}}$ have no time to decay during these oscillations. Therefore, the GWs induced by these $\phi_{\mathbf{k}}$ right after the eMD, estimated as $h \sim \mathcal{H}^{-2}\phi'\phi' \sim (k\tau_R)^2\zeta^2 \gg \zeta^2$, would be much more significant than those produced in a standard RD Universe, given by $h \sim \zeta^2$. Now let us see how the dissipation in the RD era affects this mechanism.
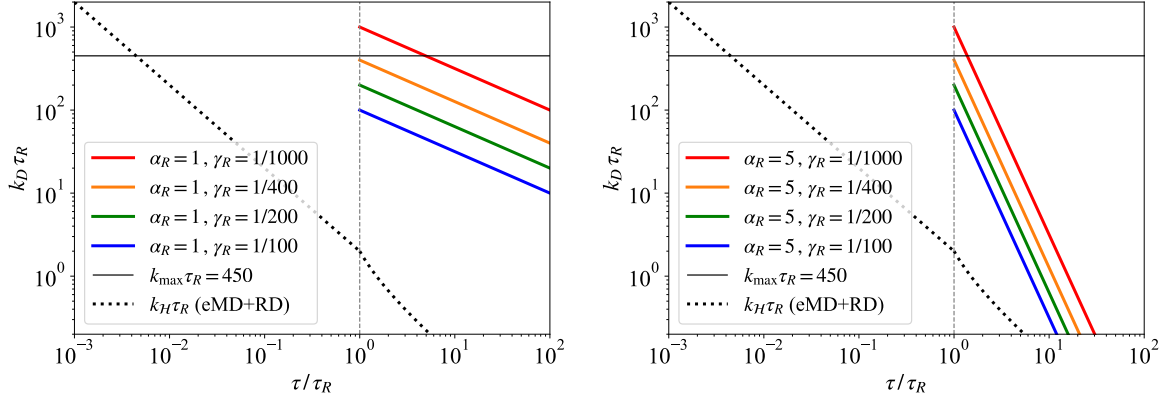

Figure 13. Damping scale k_D right after the eMD era (normalized by $1/\tau_R$) as a function of τ/τ_R for different values of α_R and γ_R. The comoving Hubble parameter $\kappa_{\mathcal{H}}\tau_R$ and the cutoff scale $k_{\max}\tau_R$ are also plotted for comparison. In the left (or right) panel, we fix $\alpha_R = 1$ (or $\alpha_R = 5$) and take $\gamma_R = 1/1000, 1/400, 1/200, 1/100$.

For different dissipation parameters α_R and γ_R, we plot the evolution of damping scale $k_D(\tau)$ in Fig. 13 and the corresponding the IGW spectra (normalized by $\mathcal{A}_\zeta^2$) caused by the poltergeist mechanism in Fig. 14. Here, we adopt $\mathcal{P}_\zeta(k) = \mathcal{A}_\zeta \Theta(k_{\max} - k)$ with the cutoff scale $k_{\max} = 450/\tau_R$. As shown in Fig. 14, while the poltergeist mechanism enhances Ω_{gw} to $\sim 10^{12}\mathcal{A}_\zeta^2$ at $k \sim k_{\max}$, dissipative effects reduce this enhancement. For $\gamma_R < 1/(k_{\max}\tau_R)$, the Ω_{gw} can be reduced by several orders of magnitude compared to the dissipation-free case,

and this reduction is highly sensitive to γ_R. The peak position shifts from $k \sim k_{\max}$ to $k \sim 1/\gamma_R$, which means that on the scales of $1/\gamma_R \lesssim k \lesssim k_{\max}$, dissipative effects suppress the IGW production more than the poltergeist mechanism enhances it. However, as long as $\gamma_R > 1/(k_{\max}\tau_R)$, dissipative effects become unimportant and do not change the magnitude of Ω_{gw}. Furthermore, by comparing the left and right panels of Fig. 14, we find that α_R can also slightly change Ω_{gw} (within one order of magnitude). These findings can be understood as follows. For $k\tau_R \gg 1$, poltergeist GWs are mainly produced in a short period after the beginning of RD era ($k\tau_R \lesssim k\tau \lesssim \mathcal{O}(1) \times k\tau_R$) [97], so the dissipative effects almost entirely depend on $k_D(\tau_R) = 1/\gamma_R$ and is not sensitive to the subsequent evolution of $k_D(\tau)$. Note that the properties of dissipative effects in the poltergeist mechanism are quite different from those in the standard RD Universe. A notable difference between these two types of IGWs production is that, the former happens deep inside the horizon (i.e., $k\tau \gtrsim k\tau_R \gg 1$), while the latter mainly happens when $\phi_{\mathbf{k}}$ just reenters the horizon (i.e., $k\tau \gtrsim 1$). Therefore, considering that dissipation is "deep-inside-the-horizon" physics, its impact on the poltergeist mechanism could be extremely significant, even when k_D is much smaller than $k_{\mathcal{H}}$. Our results indicate that dissipative effects are an important factor to consider in the poltergeist mechanism.
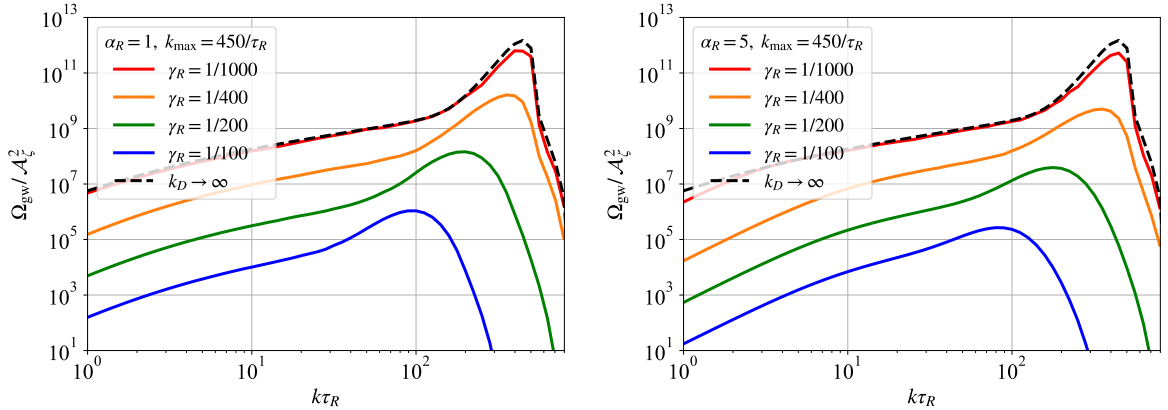

Figure 14. Energy-density spectra of IGWs (normalized by $\mathcal{A}_\zeta^2$) in the poltergeist mechanism versus the scale $k\tau_R$ with (solid lines) or without (dashed lines) dissipation. In the left (or right) panel, we fix $\alpha_R = 1$ (or $\alpha_R = 5$) and take $\gamma_R = 1/1000, 1/400, 1/200, 1/100$. In both panels, we adopt the primordial curvature power spectrum $\mathcal{P}_\zeta(k) = \mathcal{A}_\zeta \, \Theta(k_{\max} - k)$ with $k_{\max} = 450/\tau_R$.

6 Conclusions

In the early Universe, due to particle diffusion, the cosmic fluid behaves as a viscous imperfect fluid, inevitably exhibiting dissipative effects. These dissipative effects are closely related to the particle interaction in the early Universe and become especially significant near the decoupling of weakly-interacting particles. Dissipation can alter the evolution of cosmological scalar perturbations, causing their exponential damping on small scales. Since cosmological

scalar perturbations induce GWs, the impact of dissipation on their evolution inside the horizon naturally imprints onto the IGW spectrum.

Dissipative effects can introduce rich phenomenology in IGWs. Dissipation is most prominent around $\kappa \sim 1$, corresponding to the horizon scale at weakly-interacting particle decoupling. The detailed phenomenology largely depends on the shape of $\mathcal{P}_\zeta$ near $\kappa \sim 1$, as well as on the dissipation parameters α and γ. For a scale-invariant $\mathcal{P}_\zeta$, dissipative effects produce a characteristic double-valley structure in the IGWs spectrum near $\kappa \gtrsim 1$, where the positions and depths of the valleys are determined by α and γ. For a monochromatic $\mathcal{P}_\zeta$, dissipative effects smooth the original resonant peak/valley in the IGWs spectrum and modify the logarithmic infrared behavior, and these changes quantitatively depend on α, γ, and κ_ζ. For a log-normal $\mathcal{P}_\zeta$, dissipation effects combine the above two cases, featuring significant suppression near $\kappa \sim 1$ and modification of the logarithmic infrared behavior, with properties depending more complexly on α, γ, κ_ζ, and σ. All of these phenomenological features can be intuitively explained by introducing the effective "dissipation-induced" lifetimes of IGW sources.

Dissipative effects on IGWs have important implications for future GW observations. Within the SM, dissipation is dominated by neutrinos and substantially affects IGWs at nanohertz frequencies, an effect that must be considered when analyzing PTA data. If there exist weakly-interacting particles beyond the SM, their dissipation effects may leave distinctive imprints at higher frequencies in the IGW spectrum, making them important targets for future PTAs and space-/ground-based GW interferometers. In addition, the modification of the logarithmic infrared behavior and the reduction in the total GW energy density fraction caused by dissipation are also effects that must be taken into account in future GW analysis.

Dissipative effects in IGWs open an new window for probing new physics. The dissipation-induced features in the GW spectrum is characteristic imprints of weakly interacting particle decoupling and encode crucial information about their interactions. By establishing a general relation between these features (especially their frequencies) and particle interactions in the early Universe, we propose a novel paradigm to search for potential new physics via detecting dissipation effects in IGWs. This provides a new framework to explore new physics at extremely high energy scales, which enhances our capability to explore the early Universe and fundamental physics.

As an extension, we have also preliminarily discussed the dissipative effects in the presence of primordial non-Gaussianity, as well as its impact on GW anisotropies and the poltergeist mechanism. When primordial non-Gaussianity is present, the influence of dissipation near $\kappa \sim 1$ would "spread" to other scales due to mode coupling of ζ at different scales. The anisotropies of IGWs are insensitive to dissipation, as dissipation is essentially a subhorizon effect and does not alter the large-scale distribution of IGWs. The effect of dissipation on the poltergeist mechanism largely depends on the parameter γ_R. The poltergeist

GWs can be suppressed by several orders of magnitude if $\gamma_R < 1/(k_{\max}\tau_R)$, reflecting that the importance of considering dissipative effects in this mechanism.

The study of dissipative effects represents a promising direction for future GW cosmology. Given the universality of dissipation in the early Universe, it can significantly impact various mechanisms of cosmological gravitational wave production, such as those arising from cosmological phase transitions [99]. Furthermore, since dissipation originates from microscopic particle processes, its associated phenomenology is expected to bear distinctive signatures linked to particle interactions. A deeper understanding of dissipative effects not only enables more precise modeling of gravitational wave generation mechanisms but also provides a valuable bridge to deepen our insight into the early Universe and fundamental physics.

Acknowledgments

References

[1] G.M. Harry and (for the LIGO Scientific Collaboration), *Advanced ligo: the next generation of gravitational wave detectors*, *Classical and Quantum Gravity* **27** (2010) 084006.

[2] VIRGO collaboration, *Advanced Virgo: a second-generation interferometric gravitational wave detector*, *Class. Quant. Grav.* **32** (2015) 024001 [1408.3978].

[3] KAGRA collaboration, *Detector configuration of KAGRA: The Japanese cryogenic gravitational-wave detector*, *Class. Quant. Grav.* **29** (2012) 124007 [1111.7185].

[4] LIGO SCIENTIFIC, VIRGO, KAGRA collaboration, *Upper Limits on the Isotropic Gravitational-Wave Background from the first part of LIGO, Virgo, and KAGRA's fourth Observing Run*, 2508.20721.

[5] LISA collaboration, *LISA Definition Study Report*, 2402.07571.

[6] F. Jenet et al., *The North American Nanohertz Observatory for Gravitational Waves*, 0909.1058.

[7] EPTA collaboration, *The European Pulsar Timing Array and the Large European Array for Pulsars*, *Class. Quant. Grav.* **30** (2013) 224009.

[8] R.N. Manchester et al., *The Parkes Pulsar Timing Array Project*, *Publ. Astron. Soc. Austral.* **30** (2013) 17 [1210.6130].

[9] K.J. Lee, *Prospects of Gravitational Wave Detection Using Pulsar Timing Array for Chinese Future Telescopes*, in *Frontiers in Radio Astronomy and FAST Early Sciences Symposium 2015*, L. Qain and D. Li, eds., vol. 502 of *Astronomical Society of the Pacific Conference Series*, p. 19, Feb., 2016.

[10] NANOGRAV collaboration, *The NANOGrav 15 yr Data Set: Evidence for a Gravitational-wave Background*, *Astrophys. J. Lett.* **951** (2023) L8 [`2306.16213`].

[11] EPTA collaboration, *The second data release from the European Pulsar Timing Array III. Search for gravitational wave signals*, `2306.16214`.

[12] D.J. Reardon et al., *Search for an Isotropic Gravitational-wave Background with the Parkes Pulsar Timing Array*, *Astrophys. J. Lett.* **951** (2023) L6 [`2306.16215`].

[13] H. Xu et al., *Searching for the Nano-Hertz Stochastic Gravitational Wave Background with the Chinese Pulsar Timing Array Data Release I*, *Res. Astron. Astrophys.* **23** (2023) 075024 [`2306.16216`].

[14] S. Mollerach, D. Harari and S. Matarrese, *CMB polarization from secondary vector and tensor modes*, *Phys. Rev.* **D69** (2004) 063002 [`astro-ph/0310711`].

[15] K.N. Ananda, C. Clarkson and D. Wands, *The Cosmological gravitational wave background from primordial density perturbations*, *Phys. Rev.* **D75** (2007) 123518 [`gr-qc/0612013`].

[16] D. Baumann, P.J. Steinhardt, K. Takahashi and K. Ichiki, *Gravitational Wave Spectrum Induced by Primordial Scalar Perturbations*, *Phys. Rev.* **D76** (2007) 084019 [`hep-th/0703290`].

[17] H. Assadullahi and D. Wands, *Constraints on primordial density perturbations from induced gravitational waves*, *Phys. Rev.* **D81** (2010) 023527 [`0907.4073`].

[18] J.R. Espinosa, D. Racco and A. Riotto, *A Cosmological Signature of the SM Higgs Instability: Gravitational Waves*, *JCAP* **09** (2018) 012 [`1804.07732`].

[19] K. Kohri and T. Terada, *Semianalytic calculation of gravitational wave spectrum nonlinearly induced from primordial curvature perturbations*, *Phys. Rev.* **D97** (2018) 123532 [`1804.08577`].

[20] G. Domènech, *Scalar Induced Gravitational Waves Review*, *Universe* **7** (2021) 398 [`2109.01398`].

[21] NANOGRAV collaboration, *The NANOGrav 15 yr Data Set: Search for Signals from New Physics*, *Astrophys. J. Lett.* **951** (2023) L11 [`2306.16219`].

[22] PLANCK collaboration, *Planck 2018 results. VI. Cosmological parameters*, *Astron. Astrophys.* **641** (2020) A6 [`1807.06209`].

[23] S. Weinberg, *Entropy generation and the survival of protogalaxies in an expanding universe*, *Astrophys. J.* **168** (1971) 175.

[24] J. Silk, *Cosmic black body radiation and galaxy formation*, *Astrophys. J.* **151** (1968) 459.

[25] D. Jeong, J. Pradler, J. Chluba and M. Kamionkowski, *Silk damping at a redshift of a billion: a new limit on small-scale adiabatic perturbations*, *Phys. Rev. Lett.* **113** (2014) 061301 [`1403.3697`].

[26] Y.-H. Yu and S. Wang, *Silk damping in scalar-induced gravitational waves: a novel probe for new physics*, *Sci. China Phys. Mech. Astron.* **68** (2025) 210412 [`2405.02960`].

[27] G. Domènech and J. Chluba, *Regularizing the induced GW spectrum with dissipative effects*, *JCAP* **07** (2025) 034 [`2503.13670`].

[28] C. Eckart, *The Thermodynamics of irreversible processes. 3.. Relativistic theory of the simple fluid*, *Phys. Rev.* **58** (1940) 919.

[29] G.P. Lepage, *Adaptive multidimensional integration: VEGAS enhanced*, *J. Comput. Phys.* **439** (2021) 110386 [`2009.05112`].

[30] R.-G. Cai, S. Pi and M. Sasaki, *Universal infrared scaling of gravitational wave background spectra*, *Phys. Rev. D* **102** (2020) 083528 [`1909.13728`].

[31] S. Wang, T. Terada and K. Kohri, *Prospective constraints on the primordial black hole abundance from the stochastic gravitational-wave backgrounds produced by coalescing events and curvature perturbations*, *Phys. Rev.* **D99** (2019) 103531 [`1903.05924`].

[32] R. Nan, D. Li, C. Jin, Q. Wang, L. Zhu, W. Zhu et al., *The Five-Hundred-Meter Aperture Spherical Radio Telescope (FAST) Project*, *Int. J. Mod. Phys. D* **20** (2011) 989 [`1105.3794`].

[33] P.E. Dewdney, P.J. Hall, R.T. Schilizzi and T.J.L.W. Lazio, *The Square Kilometre Array*, *IEEE Proceedings* **97** (2009) 1482.

[34] K. Kuroda, W.-T. Ni and W.-P. Pan, *Gravitational waves: Classification, Methods of detection, Sensitivities, and Sources*, *Int. J. Mod. Phys. D* **24** (2015) 1530031 [`1511.00231`].

[35] LISA collaboration, *Laser Interferometer Space Antenna*, `1702.00786`.

[36] J.I. Thorpe et al., *The Laser Interferometer Space Antenna: Unveiling the Millihertz Gravitational Wave Sky*, in *Bulletin of the American Astronomical Society*, vol. 51, p. 77, Sept., 2019, DOI [`1907.06482`].

[37] LISA Cosmology Working Group collaboration, *Cosmology with the Laser Interferometer Space Antenna*, *Living Rev. Rel.* **26** (2023) 5 [`2204.05434`].

[38] W.-R. Hu and Y.-L. Wu, *The Taiji Program in Space for gravitational wave physics and the nature of gravity*, *Natl. Sci. Rev.* **4** (2017) 685.

[39] TianQin collaboration, *TianQin: a space-borne gravitational wave detector*, *Class. Quant. Grav.* **33** (2016) 035010 [`1512.02076`].

[40] N. Seto, S. Kawamura and T. Nakamura, *Possibility of direct measurement of the acceleration of the universe using 0.1-Hz band laser interferometer gravitational wave antenna in space*, *Phys. Rev. Lett.* **87** (2001) 221103 [`astro-ph/0108011`].

[41] S. Kawamura et al., *Current status of space gravitational wave antenna DECIGO and B-DECIGO*, *PTEP* **2021** (2021) 05A105 [`2006.13545`].

[42] J. Crowder and N.J. Cornish, *Beyond LISA: Exploring future gravitational wave missions*, *Phys. Rev. D* **72** (2005) 083005 [`gr-qc/0506015`].

[43] T.L. Smith and R. Caldwell, *Sensitivity to a Frequency-Dependent Circular Polarization in an Isotropic Stochastic Gravitational Wave Background*, *Phys. Rev. D* **95** (2017) 044036 [`1609.05901`].

[44] M. Punturo et al., *The Einstein Telescope: A third-generation gravitational wave observatory*, *Class. Quant. Grav.* **27** (2010) 194002.

[45] D. Reitze et al., *Cosmic Explorer: The U.S. Contribution to Gravitational-Wave Astronomy beyond LIGO*, *Bull. Am. Astron. Soc.* **51** (2019) 035 [`1907.04833`].

[46] C. Yuan, Z.-C. Chen and Q.-G. Huang, *Log-dependent slope of scalar induced gravitational waves in the infrared regions*, *Phys. Rev. D* **101** (2020) 4 [`1910.09099`].

[47] R.-g. Cai, S. Pi and M. Sasaki, *Gravitational Waves Induced by non-Gaussian Scalar Perturbations*, `1810.11000`.

[48] P. Adshead, K.D. Lozanov and Z.J. Weiner, *Non-Gaussianity and the induced gravitational wave background*, *JCAP* **10** (2021) 080 [`2105.01659`].

[49] C. Han, Z.-C. Chen, H. Yu and P. Wu, *Infrared behavior of induced gravitational waves from isocurvature perturbations*, *Phys. Rev. D* **111** (2025) 123553 [`2501.09939`].

[50] D. Luo, Y.-H. Yu, J.-P. Li and S. Wang, *Isotropic background and anisotropies of gravitational waves induced by cosmological soliton isocurvature perturbations*, *JCAP* **04** (2025) 085 [`2501.02965`].

[51] J.-P. Li, S. Wang, Z.-C. Zhao and K. Kohri, *Isotropy, anisotropies and non-Gaussianity in the scalar-induced gravitational-wave background: diagrammatic approach for primordial non-Gaussianity up to arbitrary order*, `2505.16820`.

[52] T.L. Smith, E. Pierpaoli and M. Kamionkowski, *A new cosmic microwave background constraint to primordial gravitational waves*, *Phys. Rev. Lett.* **97** (2006) 021301 [`astro-ph/0603144`].

[53] T.J. Clarke, E.J. Copeland and A. Moss, *Constraints on primordial gravitational waves from the Cosmic Microwave Background*, *JCAP* **10** (2020) 002 [`2004.11396`].

[54] A. Leike, *The Phenomenology of extra neutral gauge bosons*, *Phys. Rept.* **317** (1999) 143 [`hep-ph/9805494`].

[55] FCC collaboration, *FCC-ee: The Lepton Collider: Future Circular Collider Conceptual Design Report Volume 2*, *Eur. Phys. J. ST* **228** (2019) 261.

[56] ILC International Development Team collaboration, *The International Linear Collider: Report to Snowmass 2021*, `2203.07622`.

[57] CEPC Study Group, *CEPC Conceptual Design Report: Volume 1 - Accelerator*, `1809.00285`.

[58] CEPC Study Group, *CEPC Conceptual Design Report: Volume 2 - Physics & Detector*, `1811.10545`.

[59] S. Antusch et al., *New Physics Search at the CEPC: a General Perspective*, `2505.24810`.

[60] Pierre Auger collaboration, *The Pierre Auger Cosmic Ray Observatory*, *Nucl. Instrum. Meth. A* **798** (2015) 172 [`1502.01323`].

[61] Telescope Array collaboration, *Telescope array experiment*, *Nucl. Phys. B Proc. Suppl.* **175-176** (2008) 221.

[62] LHAASO collaboration, *The Large High Altitude Air Shower Observatory (LHAASO) Science Book (2021 Edition)*, *Chin. Phys. C* **46** (2022) 035001 [`1905.02773`].

[63] M. Braglia, X. Chen and D.K. Hazra, *Probing Primordial Features with the Stochastic Gravitational Wave Background*, *JCAP* **03** (2021) 005 [`2012.05821`].

[64] M. Kawasaki, H. Nakatsuka and I. Obata, *Generation of Primordial Black Holes and Gravitational Waves from Dilaton-Gauge Field Dynamics*, *JCAP* **05** (2020) 007 [`1912.09111`].

[65] M.H. Namjoo, H. Firouzjahi and M. Sasaki, *Violation of non-Gaussianity consistency relation in a single field inflationary model*, *EPL* **101** (2013) 39001 [`1210.3692`].

[66] J. Martin, H. Motohashi and T. Suyama, *Ultra Slow-Roll Inflation and the non-Gaussianity Consistency Relation*, *Phys. Rev. D* **87** (2013) 023514 [`1211.0083`].

[67] X. Chen, H. Firouzjahi, M.H. Namjoo and M. Sasaki, *A Single Field Inflation Model with Large Local Non-Gaussianity*, *EPL* **102** (2013) 59001 [`1301.5699`].

[68] Q.-G. Huang and Y. Wang, *Large Local Non-Gaussianity from General Single-field Inflation*, *JCAP* **06** (2013) 035 [`1303.4526`].

[69] S. Mooij and G.A. Palma, *Consistently violating the non-Gaussian consistency relation*, *JCAP* **11** (2015) 025 [`1502.03458`].

[70] R. Bravo, S. Mooij, G.A. Palma and B. Pradenas, *A generalized non-Gaussian consistency relation for single field inflation*, *JCAP* **05** (2018) 024 [`1711.02680`].

[71] B. Finelli, G. Goon, E. Pajer and L. Santoni, *Soft Theorems For Shift-Symmetric Cosmologies*, *Phys. Rev. D* **97** (2018) 063531 [`1711.03737`].

[72] Y.-F. Cai, X. Chen, M.H. Namjoo, M. Sasaki, D.-G. Wang and Z. Wang, *Revisiting non-Gaussianity from non-attractor inflation models*, *JCAP* **05** (2018) 012 [`1712.09998`].

[73] S. Passaglia, W. Hu and H. Motohashi, *Primordial black holes and local non-Gaussianity in canonical inflation*, *Phys. Rev. D* **99** (2019) 043536 [`1812.08243`].

[74] D.H. Lyth, C. Ungarelli and D. Wands, *The Primordial density perturbation in the curvaton scenario*, *Phys. Rev. D* **67** (2003) 023503 [`astro-ph/0208055`].

[75] N. Bartolo, S. Matarrese and A. Riotto, *On nonGaussianity in the curvaton scenario*, *Phys. Rev. D* **69** (2004) 043503 [`hep-ph/0309033`].

[76] M. Zaldarriaga, *Non-Gaussianities in models with a varying inflaton decay rate*, *Phys. Rev. D* **69** (2004) 043508 [`astro-ph/0306006`].

[77] D.H. Lyth, *Generating the curvature perturbation at the end of inflation*, *JCAP* **11** (2005) 006 [`astro-ph/0510443`].

[78] J. Frazer and A.R. Liddle, *Multi-field inflation with random potentials: field dimension, feature scale and non-Gaussianity*, *JCAP* **02** (2012) 039 [`1111.6646`].

[79] A. Linde, S. Mooij and E. Pajer, *Gauge field production in supergravity inflation: Local non-Gaussianity and primordial black holes*, *Phys. Rev. D* **87** (2013) 103506 [`1212.1693`].

[80] L. McAllister, S. Renaux-Petel and G. Xu, *A Statistical Approach to Multifield Inflation: Many-field Perturbations Beyond Slow Roll*, *JCAP* **10** (2012) 046 [`1207.0317`].

[81] J. Torrado, C.T. Byrnes, R.J. Hardwick, V. Vennin and D. Wands, *Measuring the duration of inflation with the curvaton*, *Phys. Rev. D* **98** (2018) 063525 [`1712.05364`].

[82] T. Bjorkmo and M.C.D. Marsh, *Manyfield Inflation in Random Potentials*, *JCAP* **02** (2018) 037 [`1709.10076`].

[83] H.V. Ragavendra, *Accounting for scalar non-Gaussianity in secondary gravitational waves*, *Phys. Rev. D* **105** (2022) 063533 [2108.04193].

[84] J.-P. Li, S. Wang, Z.-C. Zhao and K. Kohri, *Primordial Non-Gaussianity and Anisotropies in Gravitational Waves induced by Scalar Perturbations*, 2305.19950.

[85] N. Bartolo, D. Bertacca, V. De Luca, G. Franciolini, S. Matarrese, M. Peloso et al., *Gravitational wave anisotropies from primordial black holes*, *JCAP* **02** (2020) 028 [1909.12619].

[86] LISA COSMOLOGY WORKING GROUP collaboration, *Probing anisotropies of the Stochastic Gravitational Wave Background with LISA*, *JCAP* **11** (2022) 009 [2201.08782].

[87] F. Schulze, L. Valbusa Dall'Armi, J. Lesgourgues, A. Ricciardone, N. Bartolo, D. Bertacca et al., *GW_CLASS: Cosmological Gravitational Wave Background in the cosmic linear anisotropy solving system*, *JCAP* **10** (2023) 025 [2305.01602].

[88] J.-P. Li, S. Wang, Z.-C. Zhao and K. Kohri, *Complete Analysis of Scalar-Induced Gravitational Waves and Primordial Non-Gaussianities f_{NL} and g_{NL}*, 2309.07792.

[89] S. Wang, Z.-C. Zhao, J.-P. Li and Q.-H. Zhu, *Implications of Pulsar Timing Array Data for Scalar-Induced Gravitational Waves and Primordial Black Holes: Primordial Non-Gaussianity f_{NL} Considered*, 2307.00572.

[90] Y.-H. Yu and S. Wang, *Anisotropies in scalar-induced gravitational-wave background from inflaton-curvaton mixed scenario with sound speed resonance*, *Phys. Rev. D* **109** (2024) 083501 [2310.14606].

[91] J.Á. Ruiz and J. Rey, *Gravitational waves in ultra-slow-roll and their anisotropy at two loops*, *JCAP* **04** (2025) 026 [2410.09014].

[92] J. Rey, *A consistency relation for induced gravitational wave anisotropies*, 2411.08873.

[93] Y.-H. Yu and S. Wang, *Large anisotropies in the gravitational wave background from baryogenesis*, 2504.07838.

[94] R.K. Sachs and A.M. Wolfe, *Perturbations of a cosmological model and angular variations of the microwave background*, *Astrophys. J.* **147** (1967) 73.

[95] R. Allahverdi et al., *The First Three Seconds: a Review of Possible Expansion Histories of the Early Universe*, *Open J. Astrophys.* **4** (2021) astro.2006.16182 [2006.16182].

[96] K. Inomata, K. Kohri, T. Nakama and T. Terada, *Enhancement of Gravitational Waves Induced by Scalar Perturbations due to a Sudden Transition from an Early Matter Era to the Radiation Era*, *Phys. Rev. D* **100** (2019) 043532 [1904.12879].

[97] K. Inomata, M. Kawasaki, K. Mukaida, T. Terada and T.T. Yanagida, *Gravitational Wave Production right after a Primordial Black Hole Evaporation*, *Phys. Rev. D* **101** (2020) 123533 [2003.10455].

[98] M. Pearce, L. Pearce, G. White and C. Balazs, *Gravitational wave signals from early matter domination: interpolating between fast and slow transitions*, *JCAP* **06** (2024) 021 [2311.12340].

[99] H.-K. Guo, *Dissipative Effects as New Observables for Cosmological Phase Transitions*, 2310.10927.